https://doi.org/10.5194/egusphere-2026-1466
Preprint. Discussion started: 9 April 2026

A flexible methodology to evaluate natural variability in ClimaMeter

Clara Naldesi[1, 4], Nathalie Bertrand[4], Davide Faranda[1, 2, 3], and Mathieu Vrac[1]

[1]Laboratoire des Sciences du Climat et de l'Environnement, UMR 8212 CEA-CNRS-UVSQ, Université Paris-Saclay & IPSL, CEA Saclay, l'Orme des Merisiers, 91191, Gif-sur-Yvette, France
[2]London Mathematical Laboratory, 8 Margravine Gardens, London, W6 8RH, UK
[3]Laboratoire de Météorologie Dynamique/IPSL, Ecole Normale Supérieure, PSL Research University, Sorbonne Université, Ecole Polytechnique, IP Paris, CNRS, Paris, France
[4]Autorité de sûreté nucléaire et de radioprotection, PSE-ENV/SCAN/BEHRIG, F-92260, Fontenay-aux-Roses, France

Correspondence: Clara Naldesi (clara.naldesi@lsce.ipsl.fr)

Abstract. Anthropogenic climate change (ACC) is critically influencing numerous extreme events worldwide, leading to the development of rapid attribution frameworks that allow for the timely evaluation of the role of ACC in changes in the frequency and intensity of specific extreme events. ClimaMeter (Faranda et al., 2024b) is one of the tools recently developed to contextualize extreme weather events relative to climate change. ClimaMeter analyses extreme events shortly after they occur and leverages the analogue methodology for conditional attribution to evaluate whether and how events similar to the one analysed have changed in the recent climate. In order to attribute such changes to ACC, natural variability and its contribution must be quantified. In ClimaMeter, three modes of sea surface temperature variability are considered: the El Niño–Southern Oscillation, the Atlantic Multidecadal Oscillation, and the Pacific Decadal Oscillation. These three modes are considered with equal weight regardless of the event's location and type. Moreover, ACC is implicitly considered the primary factor influencing the occurrence of the event; therefore, changes not explained by natural variability modes are assumed to be attributable to ACC. Such an approach has potential limitations, which we address in this paper by proposing a refined and more flexible version, called ClimaMeter 2.0. First, we propose weighting the three modes of variability according to the strength of the teleconnection between the remote modes and the local hazards. Then, we test the hypothesis that ACC has critically influenced the observed changes by analysing long-term trends in specific quantiles of the local hazard variables. After extensive testing using pre-industrial climate simulations and observational data, we conclude that, while remaining within the same conceptual framework, ClimaMeter 2.0 provides greater flexibility and enables a more nuanced assessment of the influence of ACC on specific extreme events.

1 Introduction

There is increasing confidence that ACC has contributed to increases in the frequency and/or intensity of certain weather and climate extremes since the pre-industrial period (Seneviratne et al., 2021). For example, changes in temperature extremes

https://doi.org/10.5194/egusphere-2026-1466
Preprint. Discussion started: 9 April 2026

are directly linked to the radiative forcing associated with increased concentrations of greenhouse gases in the atmosphere, leading to global warming. Consequently, it is virtually certain that the frequency and intensity of heatwaves have increased, while those of cold extremes have decreased at the global scale since 1950. Precipitation extremes are influenced by increases in atmospheric water vapour content of approximately 7% per degree of global warming at the global scale, consistent with the Clausius–Clapeyron relation (Hartmann, 1994). At the regional scale, changes in extreme precipitation are modulated by atmospheric dynamics; nevertheless, the frequency and intensity of heavy precipitation events have likely increased at the global scale in most land regions. In this context, it is of interest to examine whether ACC has influenced the intensity or probability of specific extreme events. A precise subfield of climatology, extreme event attribution (EEA), has emerged and developed over the last twenty years to answer this question (Otto, 2017). Several methods exist in EEA, but they generally rely on comparing extremes in current climate conditions —- namely, a climate strongly influenced by human activities —- with the same extremes as they would have occurred under pre-industrial climate conditions (e.g., Jézéquel et al. (2018)). These two climate states are commonly referred to as the factual (F) and counterfactual (CF) conditions, respectively. As the counterfactual climate is generally not an observed state, EEA methodologies involve modelling it using climate models. Usually, multiple climate models under different greenhouse gas emission scenarios are exploited in EEA studies (Shepherd, 2016), thus requiring several days or weeks to be performed. In contrast, media coverage following an extreme event typically persists for only one or two days before public attention shifts to other topics. (Khaled and Mcheick, 2019). Consequently, this brief window represents the period during which media attention should be leveraged to effectively reach the public. Several initiatives have been developed to address this challenge, including World Weather Attribution (ref) and ClimaMeter (Faranda et al., 2024b) .

ClimaMeter is a platform designed to provide near-real time analysis of extremes a few hours after they occurred, putting them in the context of climate change. It currently analyses heatwaves, cold spells, heavy precipitation, windstorms and wildfires, based on the ERA5 reanalysis. Its main purpose is to provide information accessible to the general public on how the events analysed have changed in the present compared to the past. To assess the temporal evolution of extremes, ClimaMeter relies on the analogues methodology. This well-established technique in attribution science was devised by Yiou et al. (2007), and has been applied to attribute many kinds of extremes, such as droughts (Faranda et al., 2023), tropical cyclones (Bourdin et al., 2025), extratropical storms (Ginesta et al., 2022, 2024), cold spells (Cattiaux et al., 2010), heat waves (Faranda et al., 2022), derechos (Fery and Faranda, 2024), and tornado outbreaks (Faranda et al., 2022). One of the advantages of this method is that it focuses on the atmospheric circulation associated with a specific extreme event and provides insights into the dynamical processes that play a critical role in its development (Gavras-van Garderen et al., 2021). The central component of the ClimaMeter methodology is the identification of weather conditions similar to those characterising the event of interest, the so-called circulation analogues (Yiou et al., 2007; Yiou, 2014). Analogues are identified in both a historical period less affected by human activities, chosen to represent the counterfactual climate, and a recent period, representing factual climate conditions. Information on the temporal evolution of the event is obtained by evaluating significant changes between periods across the two sets of analogues. The changes are assessed in terms of circulation pattern and in terms of three meteorological hazards, which can lead to significant societal impacts: temperature, precipitation and wind speed. Such changes cannot be directly linked

https://doi.org/10.5194/egusphere-2026-1466
Preprint. Discussion started: 9 April 2026

to ACC, because the potential influence of low-frequency modes of variability must first be accounted for. A key component of the ClimaMeter methodology is therefore to assess the possible contribution of natural variability to the observed changes. Three modes of sea surface temperature (SST) variability are taken into account: the El Niño–Southern Oscillation (ENSO), the Atlantic Multidecadal Oscillation (AMO), and the Pacific Decadal Oscillation (PDO) (IPCC, 2021a; Deser et al., 2010). These modes are commonly represented by indices based on SST anomalies in characteristic regions, which track their evolution and define positive and negative phases. We use these indices to evaluate the phase of each mode associated with counterfactual and factual analogues. For each mode, if the two sets of indices differ statistically, the mode is considered to have potentially influenced the observed changes. Conversely, if factual and counterfactual analogues are not associated with different phases of modes, observed changes are attributed to ACC. This methodology enables a first assessment of the influence of natural variability, and allows to investigate whether analogues occurrence is associated to a specific phase of one or more modes of variability, and to highlight links between the modes and extreme circulations. On the other hand, it has limitations. First, the type of event and the specific region concerned are not taken into account. Indeed, in practice, the strength of the teleconnection of the variability mode (i.e., the ability of the mode to influence the climate in remote regions) is spatially heterogeneous and should depend on the hazard variable considered (IPCC, 2021a). Moreover, ClimaMeter method assumes that if the influence of the three modes cannot be proven, the observed changes can be ascribed to ACC. In other words, the default hypothesis is that ACC played a role, and the analysis seeks to challenge this assumption by evaluating the potential contribution of the modes of variability. While this hypothesis is typically the most appropriate, some phenomena (e.g. cyclones or storm) can be both affected by warmer background and by dynamical changes often producing nonlinear and local changes (Shepherd, 2014, 2016; Trenberth et al., 2015).

The main objective of the present work is to propose a more flexible and robust methodology for the quantification of the influence of natural variability, which expands the current ClimaMeter approach and addresses the potential limitations just discussed.

Specifically, we propose a new methodology that:

1. gives different weights to the modes of variability based on the strength of the teleconnection in the region affected by the event,

2. does not always implicitly rely on the assumption that climate change is critically influencing the observed changes between factual and counterfactual periods.

To structure this article, we first describe the data we use, including climate models, reanalysis and natural variability indices. The following section is devoted to a description of the current ClimaMeter methodology, including a reminder of the method and an in-depth discussion of its potential drawbacks, particularly with respect to the quantification of natural variability, which have not been addressed in other articles. We then propose a refined methodology, called ClimaMeter 2.0, which expands and generalises the original ClimaMeter while remaining within the same conceptual framework. Following this, we apply both the current and the new methodologies to stationary climate simulations for three distinct types of extremes. The parameters (e.g., duration, location) of every extreme are derived from real events that occurred in 2023 and have already been analyzed

https://doi.org/10.5194/egusphere-2026-1466
Preprint. Discussion started: 9 April 2026

within the ClimaMeter platform. We then compare the two approaches to quantifying natural variability by examining three reference real-world events based on reanalysis data. We finally discuss the advantages and limitations of the new methodology introduced, and outline potential directions for future developments.

2 Data

2.1 General Circulation Models

We focus on the pre-industrial simulations of three climate models, which represent the state of the climate in the mid-19th century before the beginning of industrialization. Both natural and anthropogenic external forcings are kept constant: volcanic aerosol is maintained at the average value recorded in the historical period (1850–2014), the solar constant is fixed at the average over the first two solar cycles of the historical simulation (1850–1873 mean), and anthropogenic forcings reflect the atmospheric composition of 1850 (Eyring et al., 2016). The only source of climate variability comes from processes internal to the model, and so it can be used to explore the unforced internal variability of the climate system.

We employ the daily sea level pressure to describe atmospheric circulation, and 2-m air temperature, precipitation, 10-m zonal and meridional wind components to account for meteorological hazards. We additionally use monthly sea surface temperature (SST) in order to compute preindustrial natural variability indices of ENSO (Bamston et al., 1997), AMO (Trenberth and Shea, 2006) and PDO (Mantua and Hare, 2002). The methodology we follow to compute them is detailed in section A.

We use three climate models that are part of the sixth phase of the Coupled Model Intercomparison Project (CMIP6, Eyring et al. (2016)). The first is the IPSL-CM6A-LR global climate model (Boucher et al., 2020) developed at the Institut Pierre-Simon Laplace (IPSL). The model has a regular horizontal resolution of 2.5°of longitude and 1.3°of latitude, over 2000 years of preindustrial control (*piControl*) simulation. We then use the CNRM-CM6-1 (Voldoire et al., 2019) general circulation model, developed by the Centre National de Recherches Météorologiques (CNRM) and Centre Européen de Recherche et de Formation Avancée en Calcul Scientifique (CERFACS), with horizontal resolution is of about 1.4°of both longitude and latitude over 500 years of *piControl* simulation. Finally, we also use the Max Planck Institute for Meteorology Earth System Model version 1.2 (MPI-ESM1.2, Mauritsen et al. (2019)). The atmosphere horizontal grid spacing is of 200 km, corresponding to a resolution of 1.9°over 1000 years of *piControl* simulation.

2.2 Reanalysis

We use the ERA5 global reanalysis (Hersbach et al., 2020) produced at the European Centre for Medium-Range Weather Forecasts (ECMWF). ERA5 has a horizontal resolution of 31 km and hourly output. We use daily data starting from 1950 (Bell et al., 2021) to present. Specifically, we exploit mean sea level pressure (ECMWF - Parameter Database, a) as a variable representing atmospheric circulation, and 2-m temperature (ECMWF - Parameter Database, b) , total precipitation (ECMWF - Parameter Database, c) and 10-m wind speed as hazard variables. To get the wind speed we combine the 10-m zonal (ECMWF - Parameter Database, d) and meridional (ECMWF - Parameter Database, e) wind components.

https://doi.org/10.5194/egusphere-2026-1466
Preprint. Discussion started: 9 April 2026

2.3 NOAA natural variability indices

We use natural variability indices to track the observed evolution over time of ENSO, AMO and PDO. The three indices are based on the spatial average of monthly SST anomalies in the characteristic region associated with the mode. To obtain the ENSO and PDO indices, SST anomalies are standardized. To isolate natural variability, the externally forced global SST trend is removed when computing the AMO and PDO indices.

The Niño 3.4 index is computed over the Niño 3.4 region ([170°W; 120°W] x [5°N; 5°S], blue rectangle in Fig. A1) as defined by Bamston et al. (1997), and is retrieved from the Royal Netherlands Meteorological Institute KNMI Climate Explorer. The AMO index is calculated as outlined by Trenberth and Shea (2006) over the North Atlantic region ([80°W; 0°E] x [60°N; 0°N], red rectangle in Fig. A1), and is also available in the KNMI Climate Explorer. The PDO index is computed over the North Pacific basin ([110°E; 255°E] x [65°N; 20°N], green rectangle in Fig. A1) as Mantua and Hare (2002), as is retrieved from the National Centers for Environmental Information (NCEI) of the National Oceanic and Atmospheric Administration (NOAA). All indices are based on NOAA Extended Reconstruction SSTs Version 5 (ERSSTv5) data (Huang et al., 2017).

3 ClimaMeter methodology

3.1 Reminder

This section summarizes the ClimaMeter methodology described in Faranda et al. (2024b) and is included here to provide the information necessary to understand the present work. The reader already familiar with it may proceed directly to section 3.2.

In practice, the ClimaMeter analysis of extreme events is based on the use of four fields from the ERA5 reanalysis: mean sea level pressure anomalies (MSLP), 2-m temperature, total precipitation, and 10-m wind speed. The event is defined by the atmospheric circulation that caused it (Fig. 1 step 1). Accordingly, we select the MSLP field on the day of the event over a region that includes the main impacts and key meteorological features. The selection of this region is based on expert knowledge. The events studied in ClimaMeter can have different durations, generally ranging from one day (e.g., convective storms) to about ten days (e.g., heatwaves). For events lasting more than one day, all fields are smoothed using a moving average over the event duration d, such that each daily value represents the mean of the preceding d days. MSLP and 2-m temperature anomalies are computed by removing the 1950-2023 daily seasonal cycle at every grid point and for every calendar day. Precipitation and wind speed are kept in their absolute values, given their noisy behavior. The dataset is then split in two periods, as represented in the second step of Fig. 1. The first part (1950-1986) is chosen to represent past, or counterfactual, climate conditions, namely a climate less affected by ACC. The second part (1987-2023) represents present, or factual, climate conditions critically affected by human influence. In every period, the best 30 circulation analogues are identified as the MSLP maps that minimize the pointwise Euclidean distance with the MSLP map of the event over the selected spatio-temporal domain (Fig. 1 step 3). A minimum temporal distance between analogues is set in order to avoid clusters of consecutive analogues. This ensures that the same meteorological event is not overrepresented in the analogues selection. Such minimum distance is expressed in days and depends on the event type and its typical duration. It is set to 3 days for short-lived

https://doi.org/10.5194/egusphere-2026-1466
Preprint. Discussion started: 9 April 2026

events (1–2 days), such as extratropical or convective storms, and to 7 days for longer-lasting events, such as heatwaves. Based on the obtained analogue dates, past and present composite maps of the analogues are created for MSLP and for the associated hazards: surface temperature, precipitation and wind speed (Fig. 1 step 4). To select significant shifts between present and past, we perform a bootstrap test: the analogues dates from the two periods are pooled together, 30 dates are randomly extracted 1000 times, and the corresponding difference maps are created. Significant grid points are identified as those with more than two standard deviations above or below the mean of the bootstrap sample.

The observed significant changes in mean sea level pressure and in the associated hazards can not be directly linked to ACC: before doing so, it is necessary to analyze the possible influence of low-frequency modes of natural variability. In the original ClimaMeter methodology, this has been done in a basic and intuitive way. Three main modes of SST variability are take into account: the ENSO, the AMO, and the PDO. These three modes of variability are chosen following the rational that they are the most important modulators of global surface temperature: ENSO at interannual time scales (Trenberth et al., 2002), and the AMO together with the PDO on multi-decadal time scales (Li et al., 2020; Wu et al., 2019; Meehl et al., 2016). The potential influence of the three modes of variability is summarized in a discrete indicator, referred to as the natural variability gauge. This gauge is based on evaluating the evolution of each individual mode between the two periods. To represent the overall phase of every mode, the counterfactual and factual distributions of the associated natural variability index on the dates of the analogues are computed (Fig. 1 steps 5 and 6). The two distributions are compared via the two-sided Cramér–von Mises (CvM) test at 0.05 significance level (Anderson, 1962), whose null hypothesis is that the two sets of indices have the same cumulative distribution. When the p-value obtained with the test is smaller than 0.05, the null hypothesis is rejected and the distributions are identified as significantly different. The physical interpretation is that, if the mode of variability has a different overall phase between the two periods, than its influence cannot be ruled out.

The value of the natural variability gauge following ClimaMeter (CM) approach is determined via the equation:

$$\textit{Gauge Value}_{\mathrm{CM}} = 0.05 + \sum_{i=\mathrm{ENSO,AMO,PDO}} 0.3 \cdot \mathbb{1}_{\geq 0.05}\,(\textit{pval}_i), \tag{1}$$

where the p-values are those coming from the CvM test, and the indicator function $\mathbb{1}_A(x)$ takes the value 1 if $x \in A$, and the value 0 if $x \notin A$.

By construction, the current ClimaMeter gauge is a discrete indicator that can only assume four values: 5%, 35%, 65%, and 95%, where low values are associated to events “Influenced by Natural Variability”, and high values to events influenced by climate change. The sign of the ACC influence is determined by comparing the sign of the observed change in the main hazard associated with the event with the sign of the event anomalies, both in the most affected region. If the signs are consistent, the gauge label is “Strengthened by climate change.” Conversely, if the signs are inconsistent (as in the case of a cold spell for which a positive change in temperature is found), it is “Weakened by climate change”.

This wording was chosen by acknowledging that, if a shift between modes of variability is detected, then natural variability may influence the occurrence of the weather pattern leading to a hazard. However, because the gauge considers only the relationship between circulation patterns and modes of natural variability, without assessing evolutions in local hazards, observed changes can still be attributed to climate change if the hazard is amplified. The gauge value depends on the p-values obtained

https://doi.org/10.5194/egusphere-2026-1466
Preprint. Discussion started: 9 April 2026

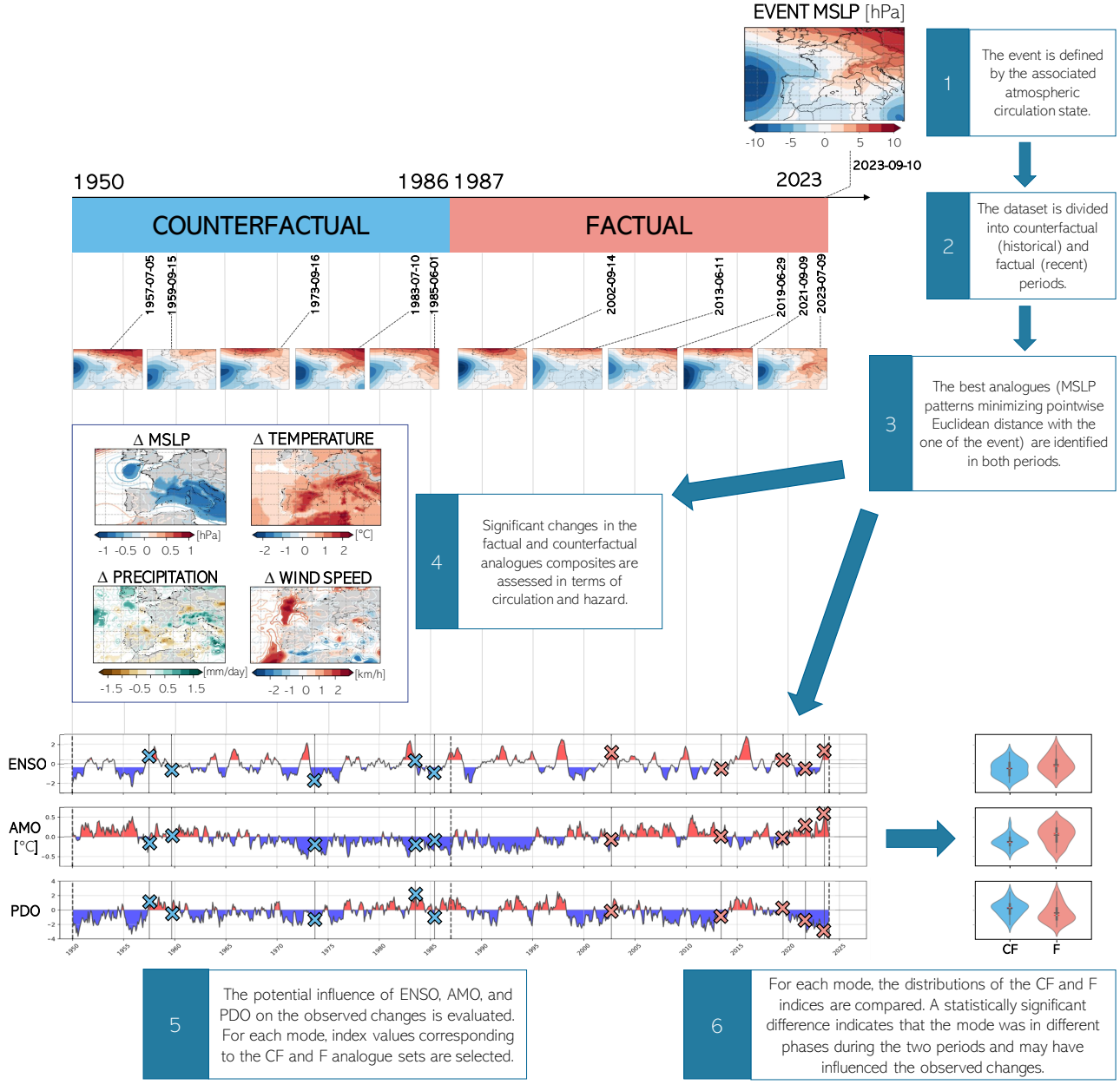

Figure 1. Schematic representation of the analogues methodology and natural variability assessment used in ClimaMeter. For space reasons, only five analogues are shown for each period, while in ClimaMeter the best 30 analogues are identified.

https://doi.org/10.5194/egusphere-2026-1466
Preprint. Discussion started: 9 April 2026

with the CvM test. As discussed above, when a p-value is smaller than 0.05, the associated mode of variability cannot be ruled out. Conversely, when a p-value is bigger than 0.05, the distributions are not significantly different and the associated mode of variability can be excluded. If none of the three p-values are bigger than 0.05, the gauge will point towards 5%, namely towards natural variability. Otherwise, the value will be increased of 30% towards climate change for every p-value bigger than 0.05. The values 0% and 100% are not used in order to take account of uncertainties in both the data and the methodology. More details and descriptions of the initial Climameter methodology can be found in (Faranda et al., 2024b).

3.2 Assumptions underlying the ClimaMeter methodology

The quantification of the influence of natural variability by ClimaMeter is based on several assumptions. The authors of ClimaMeter recognized the potential drawbacks associated with its methodology, and state that the method provides a zero-order estimate of the possible influence of natural variability (Faranda et al., 2024b). In this section, we detail the ClimaMeter working hypotheses that have not been discussed in depth in previous publications and examine their possible consequences and limitations.

1. **Limited number of SST variability modes**
   Only three low-frequency modes of SST variability are considered, and it is assumed that changes not explained by these three modes are ascribable to ACC. Choosing to represent natural variability by these three modes is a strong hypothesis: many more SST variability modes exist and are known to affect the regional occurrence of extremes. As an example, the two dominant modes of interannual climate variability in the Indian Ocean, the Indian Ocean Basin (IOB) and Indian Ocean Dipole (IOD), affect the occurrence of extremes such as heavy rainfall and heatwaves in South East and East Asia, and impact tropical cyclone formation in the western North Pacific (IPCC, 2021a; Dong et al., 2024). Additionally, the two dominant modes of tropical Atlantic variability, the Atlantic Zonal Mode (AZM) and the Atlantic Meridional Mode (AMM), are also known to influence regional and remote climate (IPCC, 2021a): the AZM has an impact on the Indian summer monsoon (Kucharski and Joshi, 2017), while the AMM is recognised to affect the Atlantic hurricane activity (Patricola et al., 2014) and tropical cyclones localised over the western North Pacific (Zhang et al., 2017). Moreover, there can be a residual variability inherent in the climate system that is not organized into any recurrent spatial pattern and, therefore, is not described by any known mode of natural variability and remains unquantified. Because of the natural variability not captured by these modes, we run the risk to incorrectly ascribing its influence on extremes to climate change.

2. **Assumption that the modes do not change because of ACC**
   Natural variability and ACC are considered as independent drivers, assuming that ACC does not affect the three modes. Current knowledge is severely limited by the fact that, although these modes have existed for millennia, confidence in paleoreconstructions of most modes prior to the instrumental era remains low (Gulev et al., 2021). Within the limits of available evidence, this hypothesis appears well founded for all three modes. For ENSO, no clear evidence indicates a recent and sustained shift beyond the range of decadal to millennial variability (Gulev et al., 2021), and there is high

https://doi.org/10.5194/egusphere-2026-1466
Preprint. Discussion started: 9 April 2026

confidence that human influence has not yet modulated its variability beyond its range of internal variability (Eyring et al., 2021). The AMO is not exhibiting any sustained change over the instrumental period [high confidence, see Bellomo et al. (2018)], and although there is robust evidence that anthropogenic and natural external forcings have modulated it over the historical period (Bellomo et al., 2018), there is low confidence in the estimated magnitude of the human influence (Birkel et al., 2018). The PDO does not show any general trend in the instrumental record (Henley, 2017), and internal variability has been its main driver (Liguori et al., 2020).

3. **No interaction between modes**

   The three modes are treated as independent and evaluated separately, while it is known that correlations between modes exist. For instance, although ENSO and PDO are two distinct modes of variability, it is recognised that the associated patterns are temporally and spatially correlated, such that El Niño (La Niña) conditions tend to coincide with the years of positive (negative) PDO phase (Mantua et al., 1997). Moreover, the AMO has been suggested to partially influence the phase of the PDO, with a negative correlation between them (Mcgregor et al., 2014).

4. **Same weight to the modes**

   Each of the three modes arbitrarily accounts for 30% of the natural variability gauge regardless of the region of the world and the hazard associated with the event. In other words, the strength of the modes' teleconnections is not quantified nor used to assign them different weights, despite it is known that remote influences are not spatially homogeneous (IPCC, 2021a).

5. **Assumption that ACC is always influencing significant changes**

   ClimaMeter always relies on the assumption that Climate Change is affecting the observed changes associated with the event. In other words, the null hypothesis that one tries to reject with the CvM test is that the CF and F sets of indices on the dates of the analogues have the same cumulative distributions; hence, that natural variability does not play a role in the observed changes. This basic assumption is acceptable for the case of temperature extremes, since we are virtually certain that the frequency and intensity of heatwaves (cold extremes) have increased (decreased) on the global scale since 1950 (Seneviratne et al., 2021). Also, at a regional scale, it is estimated that the same changes are at least likely in more than 80% of the IPCC reference regions. The case of precipitation and wind speed, however, is less spatially homogeneous, and changes are observed with a lower degree of confidence. These variables are closely related to the atmospheric circulation, and changes in dynamic aspects are not as robust as those in thermodynamics, because the large natural variability makes it difficult to identify trends (Trenberth, 2011). Heavy precipitation events are known to have increased in frequency and intensity globally, but regional variations are more heterogeneous: an increase in precipitation has been observed with medium confidence for half of the IPCC regions, while in the others, low agreement on the type of change is encountered, or limited data is available. An increase in the intensity of extreme wind has been observed in high latitudes poleward of 60°, while it is becoming less severe in the low to mid latitudes, and both changes are associated with low confidence. These considerations suggest that, although ACC is critically influencing the climate

https://doi.org/10.5194/egusphere-2026-1466
Preprint. Discussion started: 9 April 2026

system, the way it affects individual extreme events at specific locations is not straightforward, and therefore the basic assumption that ACC is the critical factor acting on changes should be tested for each case.

In the following we propose a more flexible methodology that addresses the last two potential limitations mentioned above: the equal weight given to the modes, and the assumption that climate change systematically influences the extreme under consideration. We still rely on the first three hypothesis. We do not change or increase the number of natural variability modes, even if we believe that the ClimaMeter methodology could easily be adjusted to use more than three modes of natural variability. For example, Fery and Faranda (2024) uses the analogue methodology to attribute the European derecho of 18 August 2022, and added three other modes of natural variability to the analysis: the North Atlantic Oscillation, and the East Atlantic and Scandinavian North Atlantic patterns. The same approach could easily be implemented in ClimaMeter. We still assume that natural variability modes have not changed outside natural variability because of ACC, and we consider it a reasonable hypothesis given the current state of knowledge (Gulev et al., 2021). We also continue to evaluate the modes as independent drivers and believe that it would be useful to explore the consequences of this choice in a future study.

4 ClimaMeter 2.0: an enhanced methodology to evaluate natural variability

In the present work, we aim to develop a more broadly applicable methodology to quantify the role of natural variability, with the objective of expanding the capabilities of the original ClimaMeter approach. The new method that we propose, which we refer to as ClimaMeter 2.0 or Natural Variability Gauge 2.0, has a specific focus on the local hazard associated with the event. It introduces two new features:

1. **Weighting process based on the strength of the local teleconnection**

   We compute the relative weights of the three modes based on a quantitative assessment of the teleconnection strength between the modes and the local hazard. We first define a target region, which corresponds to the area most affected by the event and in which the most extreme hazard occurred. Its boundaries are determined using a semi-objective detection approach. For each mode, we then compute the Pearson correlation ($corr$) between the time series of the natural variability index i and the local hazard X:

   $$r_i = \mathrm{corr}\Big(\mathrm{index}_i\,,\; X_{\mathrm{target}}\,\big|\mathrm{CF}\cup\mathrm{F},\,\mathrm{season}\Big), \tag{2}$$

   where X_{target} corresponds to the hazard variable of interest spatially averaged over the target region. The correlations are calculated over the union of the counterfactual (CF) and factual (F) periods, restricted to the season of interest, which depends on the event type, its typical seasonality, and its date of occurrence. We obtain the three weights – one for each index – by performing a weighted average on the absolute values of the correlation coefficients:

   $$\alpha_i = \frac{|r_i|}{\sum_{i=\mathrm{ENSO,AMO,PDO}} |r_i|}. \tag{3}$$

   The weights α_i calculated in this way provide a measure of the teleconnection between the remote modes of variability and local hazards. They allow us to assign specific, non-arbitrary magnitudes to the three modes, and address the fourth

https://doi.org/10.5194/egusphere-2026-1466
Preprint. Discussion started: 9 April 2026

limitation described in section 3.2. Also, the weighting process makes the gauge continuous ranging from 0 to 100%, providing more nuanced information.

2. **Test of the hypothesis that ACC influences observed changes**

We propose a methodology that tests whether the assumption that ACC is the critical factor influencing the observed changes between periods is valid. Fig. 2 outlines the rationale behind the approach. We focus on the evolution of the average hazard in the target region during the counterfactual and factual periods in the season of interest, and we evaluate whether there is a significant trend or not. The physical assumption we rely on and the consequent null hypothesis depend on the trend evaluation:

(a) if the trend of the hazard is significant and its sign (positive or negative) is consistent with the estimated conditional change, Δ, in the hazard over the target region given the event circulation, we hypothesize that this significant conditional change between the two periods is mainly ascribable to ACC. The null hypothesis H_0 that we test is thus that the sets of variability indices come from the same distributions, and we reject it when the associated p-value $pval$ is smaller than 0.05. This is the case assumed by ClimaMeter by default.

(b) in the other cases, i.e., a non-significant trend or a significant trend not in agreement with the sign of the conditional Δ in the hazard, our basic hypothesis is the opposite: significant changes between the two periods are mainly ascribable to natural fluctuations of the climate system. Here, the null hypothesis, that we will call $H_0{}^*$, is that the sets of variability indices come from different distributions. By analogy with the previous case, we reject $H_0{}^*$ when the associated p-value $pval^*$ is smaller than 0.05.

To compute $pval^*$, we make an approximation and state a relationship between $pval$ and $pval^*$. Statistically, a p-value is the probability that a given statistics takes a value lower than the estimated one, under the null-hypothesis. Hence, it is often intuitively interpreted as the probability that the null hypothesis is true (this is a wrong interpretation that, nevertheless, strongly eases the understanding of a statistical test). In our framework, the two null hypotheses H_0 ("*the CF and F sets of indices come from the same distribution*") and $H_0{}^*$ ("*the CF and F sets of indices come from different distributions*") are the negation of each other. As a consequence, if $pval \approx \mathbb{P}(H_0)$ and $pval^* \approx \mathbb{P}(H_0^*) = \mathbb{P}(\overline{H_0})$, then $pval^* = 1 - pval$. Using the indicator function, we can express this as: $\mathbb{1}_{\geq 0.05}\,(pval_i^*) = \mathbb{1}_{\geq 0.05}\,(1 - pval_i) = \mathbb{1}_{\geq 0.95}\,(pval_i)$. With such an approximation, the only difference between the two cases is the threshold applied to the p-values in the indicator function to statistically test the null-hypothesis:

$$thresh = \begin{cases} 0.05, & \text{if the trend in the target hazard is significant and in agreement with the conditional } \Delta \\ 0.95, & \text{otherwise.} \end{cases} \tag{4}$$

The choice of the null hypothesis is very important in the context of hypothesis testing because it defines where the burden of proof lies (Allen, 2011). The hypothesis is rejected when the statistical test exceeds the 95% confidence level in order to avoid false positives, thus favoring the null hypothesis at the expenses of the alternative hypothesis. For

https://doi.org/10.5194/egusphere-2026-1466
Preprint. Discussion started: 9 April 2026

example, if our null hypothesis is that human activity plays no role, the uncertainties of models and data will result in an underestimation of anthropogenic climate change (Trenberth, 2011). For this reason, choosing which null hypothesis is the most appropriate is a key aspect of ClimaMeter 2.0.

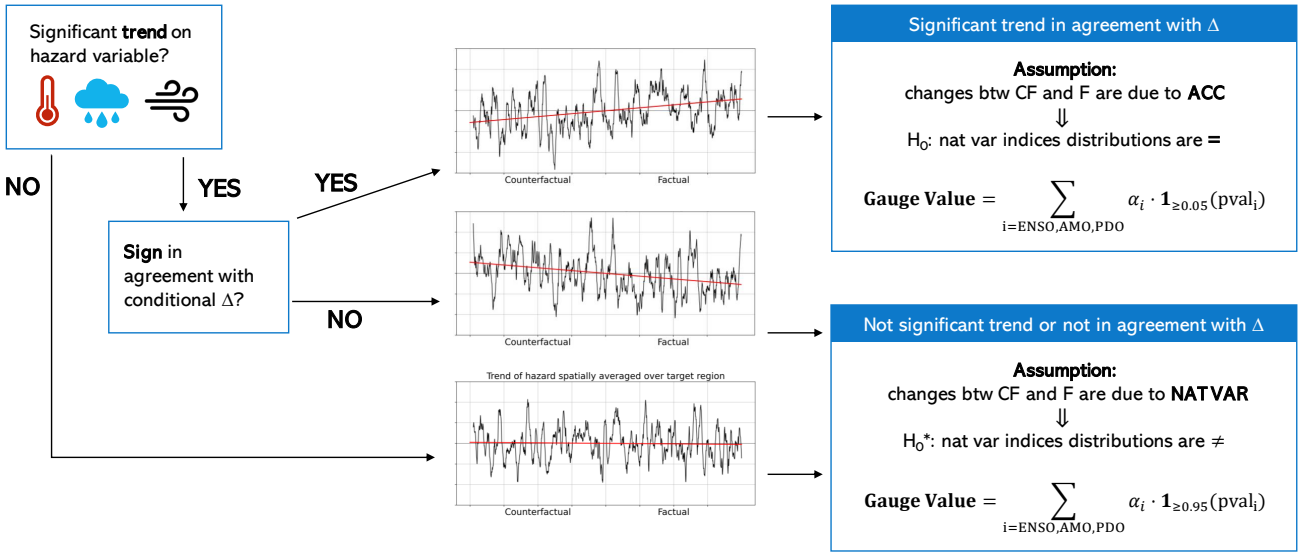

Figure 2. Scheme of the trend evaluation applied in the Natural Variability Gauge 2.0, as discussed in section 4. The trend is evaluated on the hazard variable (temperature, precipitation or wind speed) spatially averaged on the target region and during the season of interest in the counterfactual (CF) and factual periods (F). The Δ denotes the estimated change in the hazard between periods and over the target region, conditioned on the event circulation (i.e., conditioned to analogues). The blue squares summarise the two possibilities for the basic assumption and consequent null hypothesis, as well as the gauge value, based on considerations relating to the trend.

The trend in the local hazard discussed above can be computed in different ways, depending on the aspect to be highlighted. Here we propose to leverage the quantile regression technique (Koenker and Bassett, 1978) to track significant trends in specific quantiles of the local hazard distribution. The quantile regression is preferred to standard linear regression because we aim to assess changes in hazard extremes, which do not necessarily follow the behavior of the mean. For example, precipitation variability is projected to increase over land in the majority of regions (IPCC, 2021b). Global mean precipitation will very likely increase by 1–3% per °C of global surface temperature warming (Douville et al., 2021), while global increase in heavy precipitation is projected with high confidence to follow the Clausius-Clapeyron rate of about 7% per 1°C of global warming (Seneviratne et al., 2021). We suggest selecting the quantile threshold based on the hazard of the event under examination. Specifically, we compute the distribution of the hazard spatially averaged over the target region and over the union of the CF and F periods, and identify the quantile corresponding to the event hazard. We then perform the regression of that specific quantile, in order to assess whether the occurrence of events of equal or greater intensity has changes between the two periods. If the quantile associated with the event exceeds the 97^{th} quantile, we still adopt the 97^{th} quantile threshold, to ensure a sufficient sample size for a robust estimation.

https://doi.org/10.5194/egusphere-2026-1466
Preprint. Discussion started: 9 April 2026

With these additional features, the formulation for the new natural variability gauge, which we will refer to as CM 2.0 in notations, becomes:

$$\textit{Gauge Value}_{\text{CM 2.0}} = \sum_{i=\text{ENSO,AMO,PDO}} \alpha_i \cdot \mathbb{1}_{\geq thresh}\,(pval_i), \tag{5}$$

where the weights α_i are computed following Eq. (3), and the threshold $thresh$ depends on the trend evaluation, as expressed in Eq. (4).

It is important to stress that the two new features introduced in ClimaMeter 2.0 involve the timeseries of the hazard spatially averaged in the target region regardless of circulation analogues. They involve characterizing the local hazard in terms of the intensity of teleconnections of the natural variability modes and any trends that may be linked to ACC. Such characterization is unconditional to the circulation state. The link between the natural variability modes and the analogues occurrence is captured in the p-values coming from the CvM test. This was already the case in ClimaMeter, with the difference that the null hypothesis underlying the test was fixed, whereas in ClimaMeter 2.0 depends on the trend evaluation. Hence, the estimate of natural variability in ClimaMeter 2.0 contains assessments that are both conditional to the event circulation and characterizing the local hazard unconditionally. This adds important insight and makes the gauge calculation more comprehensive.

The Natural Variability Gauge 2.0 represents a broader extension with improved flexibility of the ClimaMeter approach, and both can be expressed introducing a general equation for the gauge value, formulated as a constant added to the sum of a function applied to the p-values of the three modes:

$$\textit{Gauge Value} = const + \sum_{i=\text{ENSO,AMO,PDO}} f(pval_i). \tag{6}$$

We just need to specify the right constants and functions to obtain the gauge value following ClimaMeter (Eq. 1) or ClimaMeter 2.0 (Eq. 5):

$$const_{\text{CM}} = 0.05, \qquad f_{\text{CM}}(pval_i) = 0.3 \cdot \mathbb{1}_{\geq 0.05}(pval_i), \tag{7}$$

$$const_{\text{CM 2.0}} = 0, \qquad f_{\text{CM 2.0}}(pval_i) = \alpha_i \cdot \mathbb{1}_{\geq \text{thresh}}(pval_i), \tag{8}$$

where the threshold thresh depends on the trend of the local hazard, as illustrated in Figure 2 and expressed in Eq. (4).

5 Benchmarking ClimaMeter 2.0 in a Stationary Pre-Industrial Climate

The pre-industrial experiment is conceived to evaluate the performance of the ClimaMeter 2.0 and compare it with ClimaMeter, in the reference case of a stationary climate. It is based on the pre-industrial control simulation of global climate models. Since the climate variability represented in it arises only from internal mechanisms of the climate system (Eyring et al., 2016), we expect extreme events to arise by natural variability only. The aim of the natural variability gauge is to measure to what extent specific extreme events are driven primarily by natural variability or by factors related to climate change. Accordingly, we expect extreme events occurring under pre-industrial conditions to be primarily associated with natural variability.

We performed the analysis for three climate models, obtaining consistent results. For brevity, we report here the results produced for the IPSL climate model, and those for the CNRM and MPI models are available in the supplementary materials.

https://doi.org/10.5194/egusphere-2026-1466
Preprint. Discussion started: 9 April 2026

5.1 Experiment setting

Fig. 3 depicts a scheme of the experiment for the case of pre-industrial heatwaves around Paris, which will be described in section 5.3.1. We first define the event we are interested in: its duration, typical season of occurrence, main hazard, and

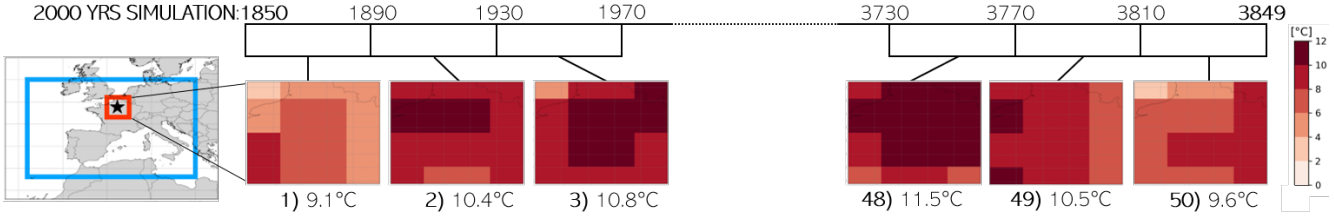

Figure 3. Scheme of the piControl experiment in the example of the pre-industrial heatwave in Paris (section 5.3.1). The 2000-year IPSL *piControl* simulation is divided in 50 blocks, each 40 years long. In every block, the target event is selected as the day with the maximum hazard (i.e. temperature anomalies) in the target region, represented by the red square, around Paris, whose location is indicated by the star. The light blue square represents the analogues region used to identify circulation analogues. The maximum temperature anomaly associated with each target is reported below the temperature anomaly plot of each target.

target region in which most extreme hazard occurred. The analogues region is consequently chosen in order to capture the meteorological features that determined the event. We preprocess the fields (MSLP, 2-m temperature, total precipitation, and 10-m wind speed) following the ClimaMeter methodology: we select the analogues region, compute a moving average across the event duration d, such that each daily value represents the mean of the preceding d days, and then select the season of interest. We divide the IPSL *piControl* run into 40-year blocks, ending up with 50 blocks. In every block we select the day for which the maximum hazard in the target region occurred. Then we consider each pair of consecutive blocks. We use the union of the two blocks as a reference period to compute mean sea level pressure, temperature, and sea surface temperature anomalies. We compute pre-industrial natural variability indices based on SST anomalies following the reference NOAA methodology, detailed in appendix A. For convenience, we compute SST anomalies on 80-years block given by the CF and F periods, while NOAA uses a 30-year period. Being in a stationary climate, we do not expect this choice to have any significant impact. We then apply the same procedure followed in ClimaMeter: we consider the first block in chronological order as counterfactual and the second as factual. The length of the blocks is chosen to be close to the actual length of counterfactual and factual periods in ClimaMeter (37 years). In each of the ClimaMeter applications, we study the target in the second, or factual, block: we look for its 30 circulation analogues in both periods separately, using mean sea level pressure anomalies patterns. We compute significant changes between the two periods in the circulation and associated hazards. We finally focus on the evaluation of natural variability following the ClimaMeter and ClimaMeter 2.0 approaches. It is worth noting that, in the ClimaMeter 2.0 method, the quantile selected for the hazard regression used to determine the threshold (Eq. 4) varies across iterations. This quantile is, in fact, defined by the target event intensity, which differs from one iteration to another. We apply this procedure to

https://doi.org/10.5194/egusphere-2026-1466
Preprint. Discussion started: 9 April 2026

each pair of consecutive blocks, that ending up with 49 outcomes of the natural variability gauge for each methodology. The long duration of the IPSL *piControl* simulation allows us to obtain a statistically significant evaluation.

The same procedure is applied to the CNRM and MPI models, and the results are available in the supplementary materials. The only difference lies in the length of the *piControl* simulations and, consequently, in the number of analogue search iterations and gauge outcomes.

5.2 Models representation of internal climate variability

The stationary experiment just discussed is devised to have a reference for the natural variability gauge in an experiment without human influence. In such context, it is important to ensure that the models we use adequately represent the three modes of natural variability.

Regarding the IPSL model, Boucher et al. (2020) evaluate the characterisation of ENSO, while Bonnet et al. (2021) assess AMO and PDO. They highlight an improved representation compared to the previous version of the model in terms of seasonality, spatial correlation, and temporal evolution.

Voldoire et al. (2019) assess the representation of the main modes of variability of the CNRM model and state that they are reasonably well simulated, with the exception of the AMO which seems to be overestimated when compared with recent observations. This is probably linked with the large AMOC variability, and the mechanism behind it is still under investigation.

Concerning MPI, Müller et al. (2018) confirm that ENSO variability is reasonably simulated in terms of periodicity and amplitude. Zanchettin et al. (2012) state that AMO and PDO are robustly captured and consistent with observed patterns.

5.3 *piControl* results

We here summarise the results obtained from the *piControl* experiment applied to the IPSL climate model. We analyse three pre-industrial events, one for every hazard: a heatwave, a summer extratropical storm associated with extreme precipitation, and a winter one associated with extreme wind speed. The choice of these events is guided by real events that have been analysed in the ClimaMeter framework. For every event, we describe its parameters and present the outcomes of the natural variability gauge, following the ClimaMeter and ClimaMeter 2.0 methodologies. All outcomes display an ensemble view of the 49 applications to the *piControl* simulation.

5.3.1 Temperature: pre-industrial heatwave in Paris

The first event we analyze is a heat wave that hits Paris and northern France. As represented in Fig. 3, the targets we select are the days with the maximum local temperature anomaly over the target region ([0°E; 5°E] x [51°N; 46.5°N]). The other parameters are chosen to be in line with the ClimaMeter study of the 2023 September European heatwave (Faranda et al., 2024a). We set a duration of 8 days, and we narrow down the analysis to summer (June to September included). To search for analogues, we use a spatial domain that includes the Eastern Atlantic and Central and Western Europe ([18°W; 20°E] x

https://doi.org/10.5194/egusphere-2026-1466
Preprint. Discussion started: 9 April 2026

[55°N; 33°N]). We impose a temporal separation between consecutive analogues of at least 7 days, in order to avoid clusters of analogues belonging to the same meteorological event.

We first perform the CvM test between the counterfactual and factual sets of natural variability indices on analogues dates. Fig. 4a-c represents the histograms of the 49 p-values coming from the CvM test, for every mode of variability. We find that in 37% of the cases the p-values associated with AMO are smaller than 5%, meaning that AMO is in different phases in the two periods and its influence can not be excluded. The impact of the AMO on European temperatures has been highlighted in several studies. For example Nicolì et al. (2020) suggest that summers in Western Europe tend to be warmer during positive AMO, while Sutton and Dong (2012) argue that a positive AMO phase is associated with hot and dry summers in western and southern Europe. For ENSO we find that the p-values are approximately uniformly distributed between 0 and 1, meaning that there is no significant occurrence of the heat wave analogues in a specific ENSO phase. The PDO is in a different phase in 27% of the iterations. The comparable magnitude of this percentage and that associated with the AMO is consistent with the existence of interbasin interactions between the two modes (Hong et al., 2022). Fig. 4d-f depicts the correlation coefficients between the average temperature anomaly in the target region and the natural variability indices (Eq. 2). We find that correlations for AMO are positive and between 0 and 0.2, while those for ENSO and PDO are centered around 0. This is again in line with literature that does not report significant teleconnections between the ENSO and PDO and anomalously warm temperatures in European summers (IPCC, 2021a). As a consequence, the weights associated to AMO are bigger than those associated to the other two modes (Fig. 4g-i).

We subsequently focus on the gauges computation, starting with the quantile regression required by the ClimaMeter 2.0 approach. Histogram in Fig. 5a represents the p-values associated with the regression. Since the null hypothesis of the test is that the regression slope is zero, p-values smaller than 5% are related to significant regressions. Slopes associated with significant trends are depicted in Fig. 5b. A significant trend in average target temperature anomalies is identified in 53% of the cases, but the proportion of significant positive trends is approximately equal to that of significant negative trends. This behaviour in *piControl* temperature variability was associated to a cycle in the Atlantic Meridional Overturning Circulation (AMOC) by Jiang et al. (2021), with a periodicity of approximately 200 years. The basic mechanism of such cycle is linked to positive anomalies in salinity in the North Atlantic, which increase convection and intensify the AMOC. This in turn causes an increase in heat transport to high latitudes and sea ice melting. The freshwater anomaly implies a negative salinity anomaly, and eventually the phase of the cycle is reversed.

Finally, we compute the 49 outcomes of the natural variability gauge following the two methodologies (Fig. 5c-d). The ClimaMeter approach classifies pre-industrial heat waves as “Influenced by Climate Change” in 51% of the times, and never recognizes them as “Influenced by Natural Variability”, namely it never points towards 5%. ClimaMeter 2.0 method, instead, gives results closer to what we would expect in an experiment without human induced climate change, identifying the vast majority of heat waves (82%) as primarily issuing from natural variability. The substantial reduction in false positives appears primarily driven by the choice of the null hypothesis based on the trend evaluation.

https://doi.org/10.5194/egusphere-2026-1466
Preprint. Discussion started: 9 April 2026

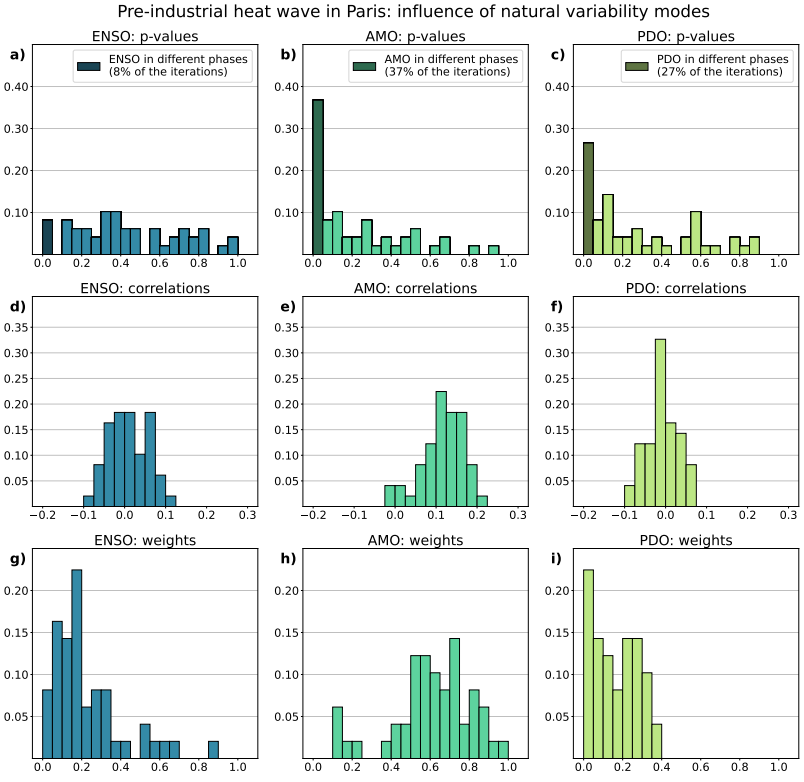

Figure 4. Pre-industrial heat wave in Paris: analysis of the influence of natural variability modes for the 49 iterations of the analogues search. The columns represents the three modes: ENSO, AMO, and PDO, respectively. The first line illustrates the results of the CvM test applied to the counterfactual and factual sets of indices on analogue dates. When the p-values is smaller than 5% we conclude that the mode was in different phases between the two periods. The second row shows the distributions of the linear correlation coefficients between the hazard, spatially averaged over the target region, and the natural variability indices, computed as expressed in Eq. (2). The third row summarizes the values of the weights computed from these correlations, calculated following Eq. (3).

5.3.2 Precipitation: pre-industrial Storm Hans

For precipitation, we choose to analyze the pre-industrial equivalent of Storm Hans, a one-day extratropical summer storm that occurred on 8 August 2023 (Messori and Faranda, 2024). The target area most impacted by extreme precipitation is Southern Scandinavia ([4.5°E; 17°E] x [63.5°N; 58°N]). The domain for the analogues selection includes Northern Europe and is centered on Scandinavia ([0°E; 30°E] x [70°N; 50°N]). We set a temporal separation between consecutive analogues of at least 3 days. We repeat the procedure described in section 5.3.1, with the difference that in this case the hazard consists of precipitation spatially averaged over the target region. Fig. 6a-b summarises the outcomes of the natural variability gauge following ClimaMeter and ClimaMeter 2.0 methodologies. The results confirm that the test of the null hypothesis introduced

https://doi.org/10.5194/egusphere-2026-1466
Preprint. Discussion started: 9 April 2026

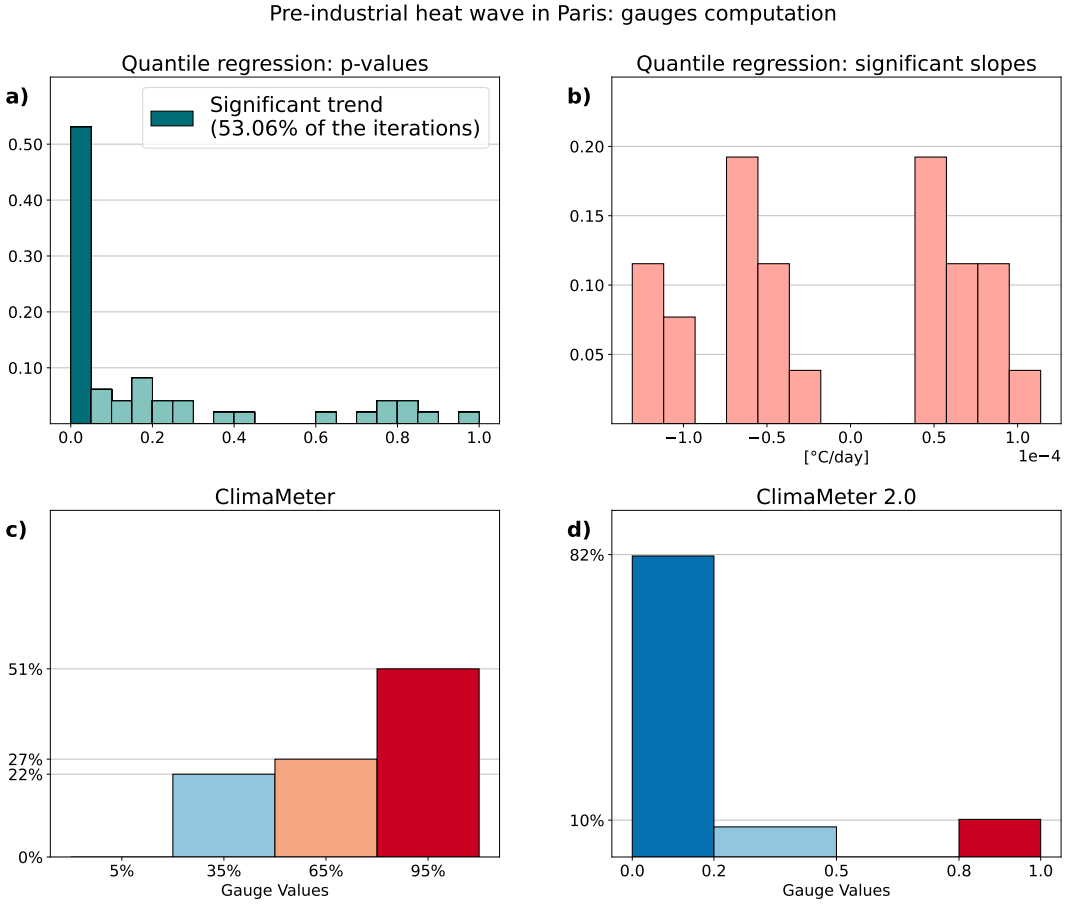

Figure 5. Pre-industrial heat wave in Paris: computation of the natural variability gauge outcomes following ClimaMeter and ClimaMeter 2.0 methodologies. All histograms represent the set of results in each iteration of the analogues search. Histogram a) represents p-values associated with the quantile regression of temperature anomalies in the target region. Since the null hypothesis of the test is that the regression slope is zero, p-values smaller than 5% (first bin in a darker shade of green) are associated with significant trends. Histogram b) depicts slopes associated with significant regressions. The second line depicts the results of the gauge following ClimaMeter and ClimaMeter 2.0 methods. Low gauge values are associated with events "Influenced by Natural Variability", while high values to events "Influenced by Climate Change". In histogram d), bin limits are chosen so as to have the minimum distance between the possible values of the original ClimaMeter gauge.

https://doi.org/10.5194/egusphere-2026-1466
Preprint. Discussion started: 9 April 2026

in ClimaMeter 2.0 leads to a radical drop of pre-industrial storms related to Climate Change. The intermediary steps needed for the gauges computations (weights and trends, as shown for the heat wave) are available as supplementary materials.

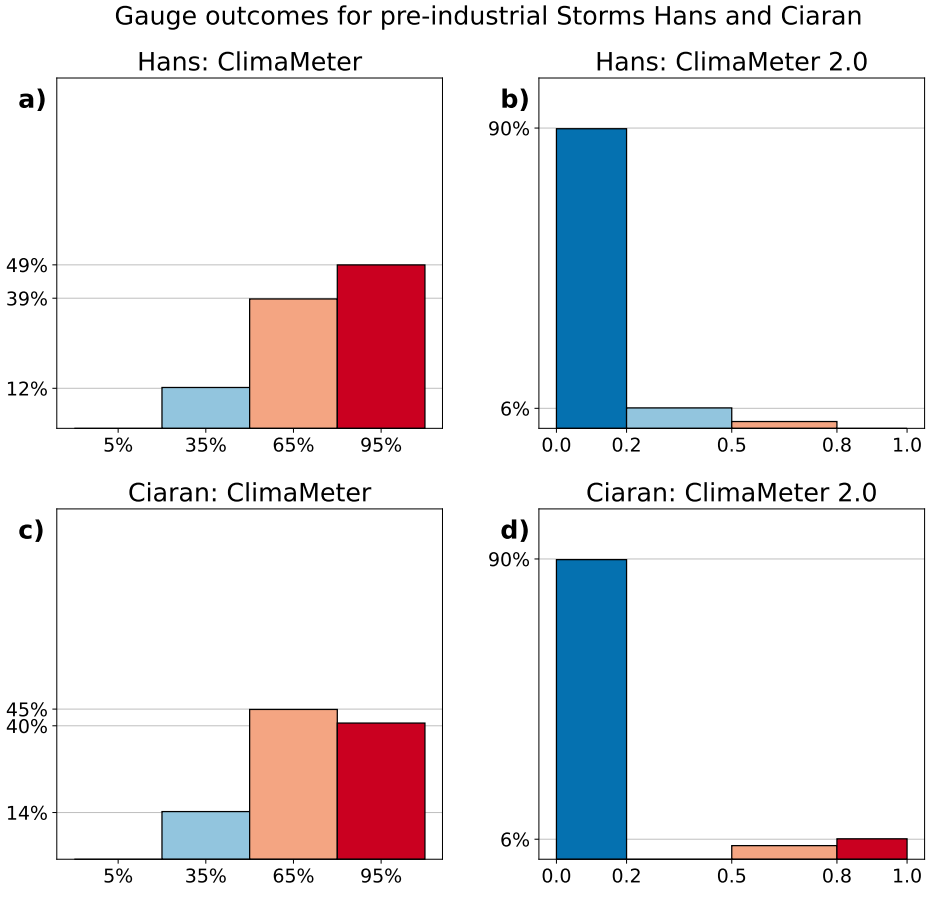

Figure 6. Pre-industrial storms Hans and Ciaran: outcomes of the natural variability gauge for every iteration following ClimaMeter (first column) and ClimaMeter 2.0 (second column) methodologies. Low gauge values are associated with events "Influenced by Natural Variability", while high values to events "Influenced by Climate Change". The first line refers to Storm Hans (section 5.3.2), while the second for Storm Ciaran (section 5.3.3). The events have the same parameters of real storms Hans (Messori and Faranda, 2024) and Ciaran (Alberti and Faranda, 2024) occurred in 2023.

5.3.3 Wind: pre-industrial Storm Ciaran

As an event associated with high wind speed, we study the pre-industrial equivalent of Storm Ciaran (Alberti and Faranda, 2024). This extratropical cyclone occurred between 2 and 3 November 2023 and caused extremely high wind speed along the entire French Atlantic coast, affecting a very large target area ([5°W; 2.5°E] x [51.2°N; 43°N]). The analogues are selected

https://doi.org/10.5194/egusphere-2026-1466
Preprint. Discussion started: 9 April 2026

during fall (September to December) and over a region covering Europe and the eastern Atlantic ([18°W; 30°E] x [65°N; 35°N]), in order to capture the low pressure center passing over Europe. We impose a temporal separation between consecutive analogues of at least 3 days. The gauges results are in substantial agreement with the two cases discussed before, with a strong decrease of false positives in ClimaMeter 2.0 (Fig. 6c-d). Outcomes of weights and regressions are available as supplementary materials.

6 Application of ClimaMeter 2.0 to Real-World Extreme Events from reanalysis data

In this section, we now analyse, within ERA5 reanalyses, the three real events that we used as a reference in the pre-industrial experiment. For each of them, we compute the outcome of the natural variability gauge following the ClimaMeter 2.0 approach, and compare with the original ClimaMeter. The analysis follows the procedure outlined in section 3.1: we perform the analogues search in the counterfactual (1950-1986) and factual (1987-2023) periods from the ERA5 reanalysis. Unlike the pre-industrial cases, we do not iterate the operation several times, and therefore we obtain only one gauge value for every methodology.

6.1 Temperature: 2023 September European Heatwave

From the 3rd to the 10th of September 2023, Southern and Central Europe experienced a period of anomalous heat. Focusing on France, 4 September has been the hottest day ever observed in September, and several records have been broken for both daily maximum and minimum temperatures (METEO FRANCE, b). On average, the vast majority of France experienced temperature anomalies of 5 to 7°C, as depicted in Fig. 7b. In line with the pre-industrial heatwave, we select the area centered over Paris as target region, where anomalies were up to 9° occurred (black square in Fig. 7b). The atmospheric circulation was in a configuration of omega blocking (Fig. 7a), with relatively low pressures over the Eastern Atlantic and the Eastern Mediterranean, and relatively high pressure over Central and Eastern Europe. Such a pattern is well known to be associated to heatwaves over Europe, since warm air coming from lower latitudes is advected towards Europe and is blocked there, possibly persisting for days (Pfahl and Wernli, 2012).

We compute circulation analogues of the event, and evaluate significant changes in temperature, shown in Fig. 7c. As expected, an increase up to 2°is found in most parts of the area, notably over the Mediterranean and Atlantic regions. Specifically, the average change in the target region is 0.86°. To assess if such changes are associated to climate change, we compute the natural variability gauge. Fig. 7e-f represents the outcomes of the natural variability gauge following the ClimaMeter and ClimaMeter 2.0 methodologies. Low values of the gauges identify events “Influenced by Natural Variability”, while high values events “Strengthened by Climate Change”. The discontinuous coloring of the ClimaMeter gauge reflects that it is a discrete indicator which can only take four values (5%, 35%, 65%, and 95%). The representation of the gauge 2.0, instead, involves a continuous coloring reflecting the continuous nature of the new gauge. The horizontal bar in Fig. 7g represents the weights associated to the three modes based on the correlation between the hazard in the target region and the natural variability indices, as expressed in Eq. (3). The p-values reported below the weights are the result of the comparison between the counterfactual

https://doi.org/10.5194/egusphere-2026-1466
Preprint. Discussion started: 9 April 2026

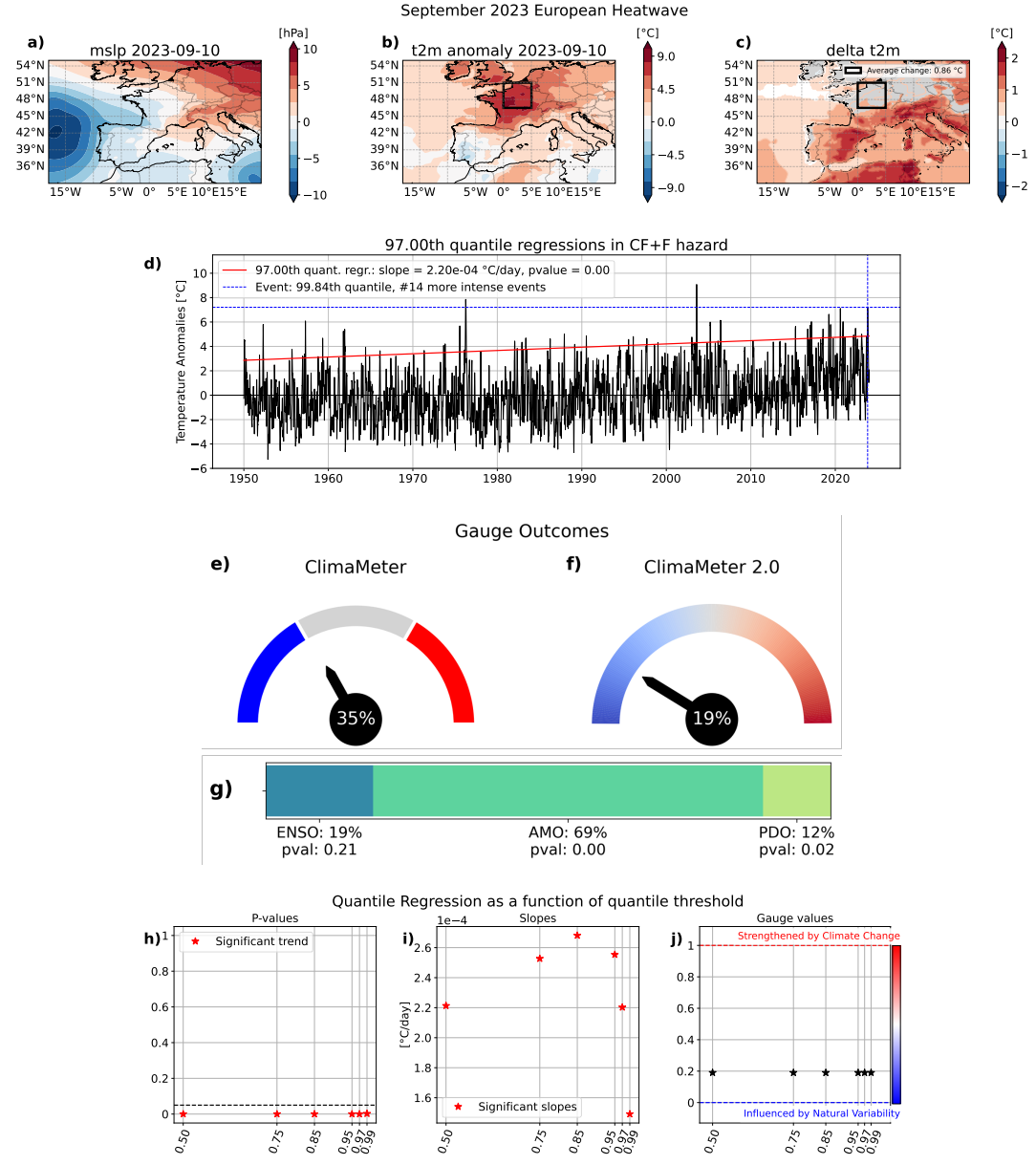

Figure 7. Analysis of the September 2023 European heatwave. (a) mean sea level pressure and (b) temperature anomalies maps associated with the event, both averaged over the heatwave duration, from 3 to 10 September. (c) Significant changes in temperature between factual and counterfactual analogues composites. Fields in a-c) cover the analogues domain ([18°W; 20°E] x [55°N; 33°N]). The black square in b) indicates the target region around Paris ([0°E; 5°E] x [51°N; 46.5°N]) where most extreme hazard and impacts occurred. d) Time evolution of temperature anomalies spatially averaged in the target region over the union of counterfactual and factual periods. The blue horizontal dashed line represents the temperature anomaly associated with the event, while the vertical the time of occurrence. The legend indicates the quantile corresponding to the event intensity within the distribution of target temperature anomalies, as well as the number of previous events with higher intensity. The red line represents the 97^{th} quantile regression of temperature anomalies, and slopes and p-values are reported in the legend. Note that a p-value smaller than 5% is associated to a significant trend, since the null hypothesis of the test is that the regression slope is zero. e-f) Comparison of natural variability gauge outcomes following ClimaMeter and ClimaMeter 2.0 methodologies. g) Weights expressed as percentages for the modes of variability, and p-values obtained from the CvM test at 0.05 significance level between counterfactual and factual set of indices. h-j) Quantile regression for different values of the quantile threshold: 0.5, 0.75, 0.85, 0.95, 0.97, 0.99. i) p-values and j) slopes associated with the regression; k) natural variability gauge value based on the quantile regression methodology, all as a function of the quantile threshold.

https://doi.org/10.5194/egusphere-2026-1466
Preprint. Discussion started: 9 April 2026

and factual sets of indices on the dates of the analogues via the CvM test. As discussed, when a p-value is greater than a specific threshold, we interpret the mode as being in the same phase between the two periods and thus we can rule out their potential influence on the observed changes. The value of the threshold depends on the methodology we follow to compute the gauge: in the ClimaMeter method, the threshold is always 5% (Eq. 1), while in ClimaMeter 2.0 it depends on the significance of the hazard trend (Eq. 4).

As shown in Fig. 7e, the ClimaMeter gauge gives a values of 35%. Specifically, the AMO and the PDO are in different phases in the two periods. To compute the values of the ClimaMeter 2.0, we first compute the quantile that corresponds to the event intensity (blue horizontal dashed line in Fig. 7d) within the distribution of temperature anomalies in the target region. This heatwave was particularly intense and lies in the 99.84^{th} quantile, with its intensity exceeded on only 14 other days since 1950. Following the methodology described in section 4, we select the 97^{th} quantile to perform the quantile regression of temperature anomaly, to avoid using an excessively small dataset. As expected in a warming climate, the regression (red line in Fig. 7d) is significant and associated to a positive slope. This is in line with a large number of studies that state that frequency and intensity of temperature extremes have increased virtually across the whole of Europe, and such increase is attributable to anthropogenic forcings with high confidence (IPCC, 2021b; Christidis and Stott, 2016). Since the regression is significant, the ClimaMeter 2.0 gauge is computed with a threshold on p-values of 5% (Eq. 4). Specifically, since only ENSO is in the same phase between the two periods and is the only mode whose influence can be neglected, the values of the gauge is equal to the weight associated to ENSO (Eq. 5), that is 19%.

We also analyzed the influence of the quantile threshold on the regression and the gauge value, as shown in Fig. 7h-j. We notice that the trend is positive and significant for all quantiles (p-values smaller than 5%). In fact, not only the extremes but also average temperatures are rising in France, with a mean increase relative to pre-industrial levels of 1.9°C in 2024, according to Meteo France estimates (METEO FRANCE, c). As a consequence, the gauge value is constant throughout quantiles.

6.2 Precipitation: Storm Hans

On 8 August 2023, the Scandinavian countries were affected by the passage of the summer extratropical storm Hans. More than 60 mm of rain were recorded in Central and Southern Sweden (black square in Fig. 8b), breaking August precipitation records in several stations (Swedish Meteorological and Hydrological Institute). Fig. 8a shows the associated circulation pattern, consisting of a low-pressure centre located over Southern Scandinavia. Significant changes in precipitation between the two periods exhibit an increase up to 6 mm/day over Central Scandinavia, and an average increase of 1.5 mm/day in the target region (Fig. 8c).

While PDO is in the same phase between the analogue days of the two periods, ENSO and AMO are not, and so they are possibly influencing the observed changes (p-values in Fig. 8g). The ClimaMeter gauge therefore points towards 35%, as depicted in Fig. 8e. Fig. 8d displays the evolution of precipitation spatially averaged over the target region. Storm Hans is an event of unprecedented intensity, as shown by the blue horizontal dashed line. As a consequence, the regression on the local hazard is performed on the 97^{th} quantile, and points out a significant increase in extreme precipitation. This is in line with the latest IPCC assessment, that states with at least medium confidence that Northern Europe is experiencing an observed increase

https://doi.org/10.5194/egusphere-2026-1466
Preprint. Discussion started: 9 April 2026

in heavy precipitation from 1950s to the present, and such observed increase can be attributed to human contribution with high confidence (IPCC, 2021b). The ClimaMeter 2.0 gauge is computed using a threshold on the p-values of 5%, and since the PDO is the only mode in the same phase and is associated to a weight of 67%, the resulting gauge value is 67%. From the analysis of the quantile regression as a function of the quantile threshold, we notice that the trend in precipitation is only significant for the high quantiles, equal to or greater than 0.95 (Fig. 8h). When the trend is significant, the associated slope is positive (Fig. 8i), confirming the increase in extreme precipitation in the region. Consistently, the gauge value based on the quantile regression points towards 67% only for high quantiles (Fig. 8j).

6.3 Wind: Storm Ciaran

Between 2 and 3 November 2023, the explosive extratropical cyclone Ciaran reached Northwestern Europe, causing extreme winds in France, the English Channel and Western Italy. The entire French Atlantic coast was affected by the event, with average winds between 40 and 60 km/h throughout its duration (black square in Fig. 9b). Wind gusts up to more than 150 km/h were recorded on the Brittany coast, breaking absolute records in several weather stations (METEO FRANCE, a). The event weather pattern depicted in Fig. 9a shows a low pressure system located over Great Britain with anomalies exceeding 30 hPa. The analysis of significant changes in wind speed between factual and counterfactual analogues points to an increase over the English Channel and Brittany, with an average increase of 3.09 km/h in the target region (Fig. 9c).

In terms of the potential influence of natural variability, only the PDO was in a different phase between the two periods (p-values in Fig. 9g) and the ClimaMeter gauge points towards 65% (Fig. 9e). Even though Storm Ciaran broke several local records, the average wind speed over the target region was exceeded on 56 days since 1950 (Fig. 9d). This is likely due to the particularly large target region, for which spatial averaging of wind speed can substantially smooth extreme values. Still, since the event corresponds to the 99.38^{th}quantile of the target wind speed distribution, we compute the 97^{th} quantile regression of wind speed, represented by the red line in Fig. 9d. Unlike the two previous cases, the regression is not significant. This agrees with the general absence of a clear observed increase in the frequency or intensity of strong winds or storms in recent decades in France (Soubeyroux et al., 2024). In this case, the threshold on p-values is 95%, and since all p-values are smaller the ClimaMeter 2.0 gauge will point towards 0% (Fig. 9f). The interpretation of such result is that, for this specific event, natural variability seems to be the determining factor that led to its occurrence. It is important to stress that such statement is only valid for storm Ciaran, its dynamics and associated wind speed, and cannot be generalised to any other storm or event.

Fig. 9h shows the significance of the trend in average target wind speed as a function of the quantile. Interestingly, it highlights that the regression is significant up to the 85^{th} quantile, meaning that average wind speed exhibits a significant increase (Fig. 9i). In such cases, the ClimaMeter 2.0 gauge depicted in Fig. 9j is equal to 83%.

7 Conclusions and perspectives

This work builds on the ClimaMeter approach for the rapid analysis of extreme events and focuses on fundamental aspects of its methodology. Specifically, ClimaMeter assesses how events with the same dynamics as the event under consideration have

https://doi.org/10.5194/egusphere-2026-1466
Preprint. Discussion started: 9 April 2026

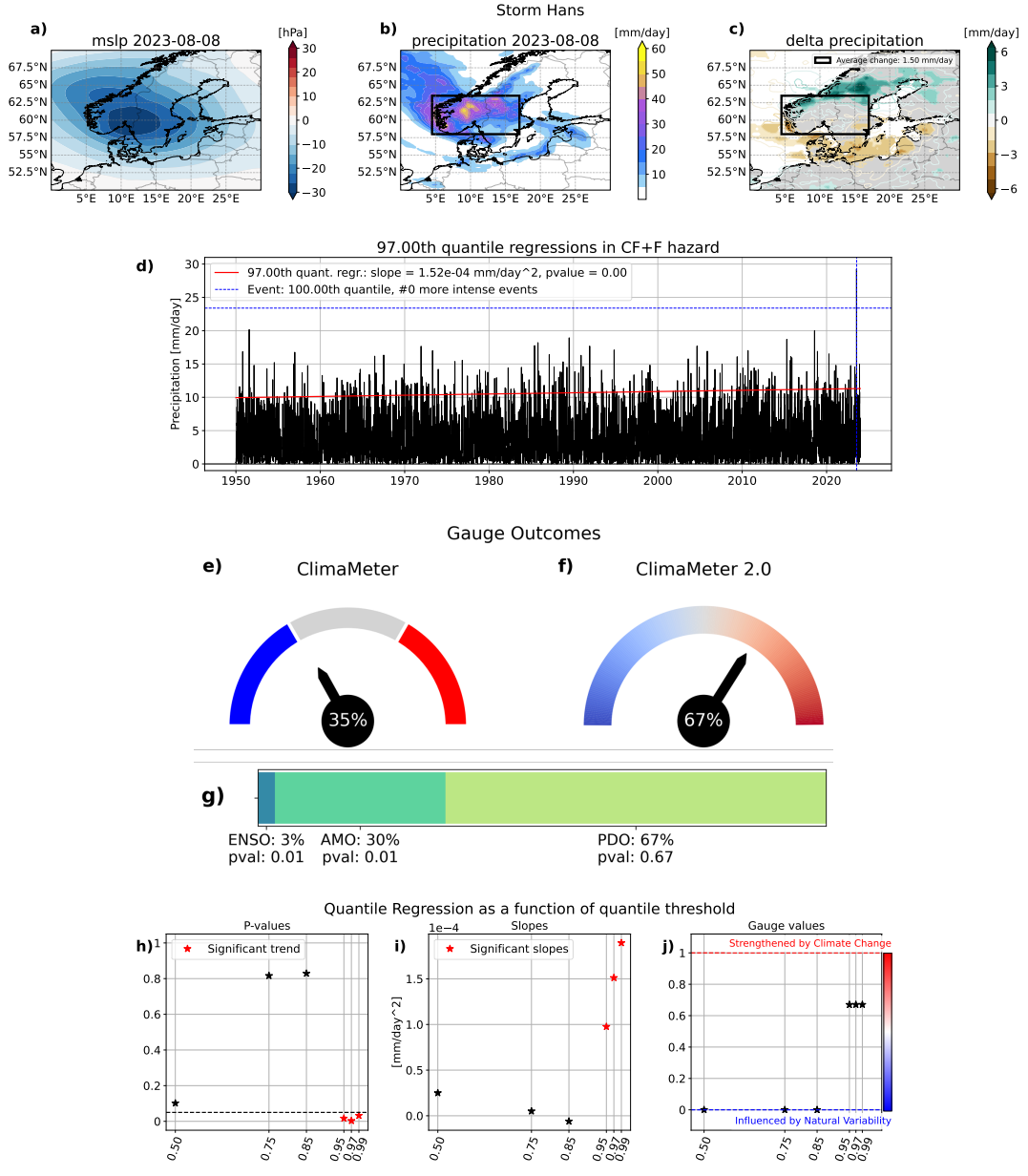

Figure 8. Analysis of Storm Hans. (a) Mean sea level pressure anomalies and (b) precipitation maps associated with the event. (c) Significant changes in precipitation between factual and counterfactual analogues composites. Fields in a-c) cover the analogues domain ([0°E; 30°E] x [70°N; 50°N]). The black square in b) indicates the target region ([4.5°E; 17°E] x [63.5°N; 58°N]) where most extreme hazard and impacts occurred. d) Time evolution of precipitation spatially averaged in the target region over the union of counterfactual and factual periods. The blue dashed line represents the precipitation associated with the event. The legend indicates the quantile corresponding to the event intensity within the distribution of the target precipitation, as well as the number of previous events with higher intensity. The red line represents the 97^{th} quantile regression of precipitation, and slopes and p-values are reported in the legend. Note that a p-value smaller than 5% is associated to a significant trend, since the null hypothesis of the test is that the regression slope is zero. e-f) Comparison of natural variability gauge outcomes following ClimaMeter and ClimaMeter 2.0 methodologies. g) Weights expressed as percentages for the modes of variability, and p-values obtained from the CvM test at 0.05 significance level between counterfactual and factual set of indices. h-j) Quantile regression for different values of the quantile threshold: 0.5, 0.75, 0.85, 0.95, 0.97, 0.99. i) p-values and j) slopes associated with the regression; k) natural variability gauge value based on the quantile regression methodology, all as a function of the quantile threshold.

https://doi.org/10.5194/egusphere-2026-1466
Preprint. Discussion started: 9 April 2026

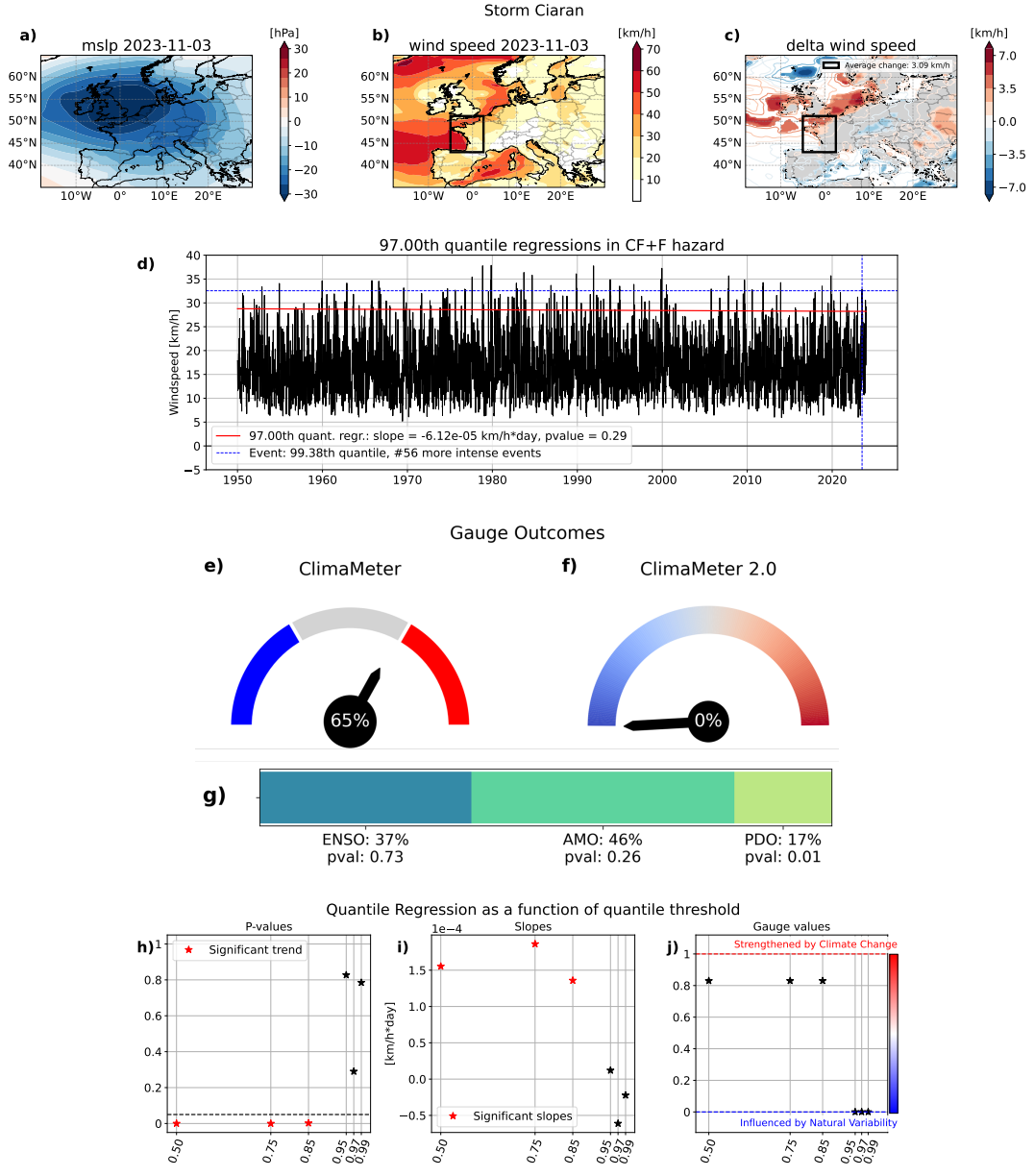

Figure 9. Analysis of Storm Ciaran. (a) Mean sea level pressure anomalies and (b) wind speed maps associated with the event. (c) Significant changes in wind speed between factual and counterfactual analogues composites. Fields in a-c) cover the analogues domain ([18°W; 30°E] x [65°N; 35°N]). The black square in b) indicates the target region ([5°W; 2.5°E] x [51.2°N; 43°N]) where most extreme hazard and impacts occurred. d) Time evolution of wind speed spatially averaged in the target region over the union of counterfactual and factual periods. The blue dashed line represents the wind speed associated with the event. The legend indicates the quantile corresponding to the event intensity within the distribution of the target wind speed, as well as the number of previous events with higher intensity. The red line represents the quantile regression of wind speed, and slopes and p-values are reported in the legend. Note that a p-value smaller than 5% is associated to a significant trend, since the null hypothesis of the test is that the regression slope is zero. e-f) Comparison of natural variability gauge outcomes following ClimaMeter and ClimaMeter 2.0 methodologies. g) Weights expressed as percentages for the modes of variability, and p-values obtained from the CvM test at 0.05 significance level between counterfactual and factual set of indices. h-j) Quantile regression for different values of the quantile threshold: 0.5, 0.75, 0.85, 0.95, 0.97, 0.99. i) p-values and j) slopes associated with the regression; k) natural variability gauge value based on the quantile regression methodology, all as a function of the quantile threshold.

https://doi.org/10.5194/egusphere-2026-1466
Preprint. Discussion started: 9 April 2026

changed from the mid-twentieth century to the present day. Before ascribing these changes to ACC, the possible role of natural variability must be assessed. The new methodology we present, the ClimaMeter 2.0 approach, proposes an enhanced way to measure the influence of natural variability on the observed changes.

ClimaMeter 2.0 represents a generalisation and extension of the original approach, while remaining within the same conceptual framework. The most important advancement lies in its improved flexibility. First, we quantify the influence of every mode of SST variability - ENSO, AMO, PDO - on the local hazard variable, namely temperature, precipitation or wind speed in the target region most affected by the event. We achieve this by computing the temporal correlation between the index associated with each mode and the hazard variable spatially averaged over the target region. We use the resulting correlation coefficients to weight the strength of each mode's teleconnection with the local hazard. The main advantages of this new feature are that the weights of the three modes are no longer assumed to be equal and that the natural variability indicator becomes continuous. Another key improvement in terms of versatility concerns the underlying hypothesis regarding the dominant factor driving the observed changes. In ClimaMeter, ACC is assumed by default to be the determining factor, and the role of natural variability must then be proved. In ClimaMeter 2.0, we propose to choose the most appropriate null hypothesis by considering the temporal evolution of the local hazard, specific to each event. We compute a quantile regression of the local hazard during the union of the counterfactual and factual periods. The relevant quantile is selected as the one corresponding to the event anomaly within the local hazard distribution. The quantile regression allows us to evaluate if events of equal or greater intensity exhibit a significant trend, and if such a trend is detected and is consistent with the observed changes, we assume that ACC plays a critical role in the event. Conversely, if no significant trend is found, the null hypothesis is that natural variability is the main factor leading to it. This procedure increases the robustness of the methodology, since the null hypothesis is explicitly tested rather than assumed. Moreover, it enhances its flexibility and can be easily adapted to any null hypothesis considered more appropriate. In fact, our assessment of ACC using quantile regression is only one possibility, and this methodology can be modified to accommodate other hypotheses. The application of the ClimaMeter 2.0 methodology to pre-industrial events gives promising results, since in most cases it identifies them as influenced by natural variability. Moreover, this result is robust across the three models analyzed, providing strong evidence for the robustness of the new method. ClimaMeter 2.0, when applied to reanalysis data, modifies the value of the previous gauge, shifting it toward either natural variability or climate change depending on the event considered. In addition to the weights assigned to the variability modes, the crucial factor determining this shift is the presence or absence of a statistically significant trend in the hazard variable.

However, the new methodology still has limitations. First, the weighting process requires taking the absolute values of the correlation coefficients between the modes and the hazards (Equation (3)). While this approach captures the magnitude of the correlations, it looses information about their sign. Each mode of variability exerts both positive and negative influences on remote climates depending on the geographical region considered (IPCC, 2021a; Deser et al., 2010). However, at the current stage, correlations of equal magnitude but opposite sign cannot be distinguished. As a result, even in cases where the correlation has the opposite sign to the observed changes, the corresponding mode is still considered as potentially influencing those changes. Incorporating the correlations sign in future developments of this work would provide a more comprehensive

https://doi.org/10.5194/egusphere-2026-1466
Preprint. Discussion started: 9 April 2026

understanding, as each mode of variability exerts both positive and negative influences on remote climates depending on the geographical region considered.

Moreover, in its current form, ClimaMeter 2.0 allows only one hazard variable to be considered at a time. Extending the framework to account for multiple local hazards would be of great interest. As an example, events like extratropical and tropical cyclones are typically associated with extremes in both precipitation and near-surface wind speed. Hence, accounting for the 2 variables when investigating the trend should provide more representative results.

Also, in ClimaMeter 2.0 we base the choice of the null hypothesis on the evaluation of a trend in the local hazard, and assume that a significant trend can be ascribed to climate change. This represents a strong assumption, since the complex effect of human influence on meteorological hazards is not necessarily well represented by a trend. As discussed above, this methodology is conceived to be flexible and easily adaptable to new choices of the null hypothesis that may be proposed in future work.

Future directions for this work involve the investigation of the consequences of the assumptions detailed in section 3.2, which are not addressed in this study. In particular, we believe it would be worthwhile to increase the number of modes of variability considered, or to select them based on their relevance to the event under consideration. The ClimaMeter 2.0 approach can be readily expanded in this direction, following, for example, the work of Fery and Faranda (2024). However, as discussed in Section 3.2, representing natural variability using recurrent SST or circulation patterns remains an approximation, and a residual component of unexplained variability will inevitably persist. Quantifying this residual contribution and explicitly including it into the gauge value computation would substantially improve the robustness of the assessment.

Moreover, including a measure of the correlation between modes of variability would allow for a more accurate quantification of their interactions and of the complex mechanisms contributing to extreme events, by that further enhancing the flexibility and level of detail of the methodology.

The new features introduced in ClimaMeter 2.0 also enable a broader range of applications. For example, the weighting process provides a quantitative measure of the influence of modes of natural variability, offering insights into how extreme events are affected by natural variability alone when the framework is applied to counterfactual periods. Furthermore, because in quantile regression the quantile threshold is directly associated with the hazard of the event under consideration, the framework is also applicable to non-extreme events. Specifically, the methodology could be readily integrated into the analyses provided by ClimaMonitor, a recent extension of ClimaMeter available on the ClimaMeter website. ClimaMonitor examines European weather conditions on a daily basis, thus representing the daily version of ClimaMeter. The new assessment of the influence of natural variability could be easily implemented within this framework, further confirming its flexibility.

Finally, an important direction for future research concerns the definition of the target region most affected by the event. In this work, the target region is identified using a semi-objective approach and is assumed to have a rectangular shape for convenience. Consequently, it includes areas affected by extreme hazards, but may also include regions experiencing more moderate conditions. For example, in the case of Storm Ciaran, extreme wind speeds were confined mainly to coastal areas of France, while inland values were substantially lower but still included within the target region (black square in Fig. 9). An interesting development could be to automatically select the target region by defining grid-points where the hazard is

https://doi.org/10.5194/egusphere-2026-1466
Preprint. Discussion started: 9 April 2026

overcoming a certain threshold. The choice of the target region is critical, as it is subsequently used to estimate trends in the hazard variable. Automating this step would represent a great improvement, specifically for variables like precipitation and wind speed, that can often be intense on a very local scale.

Appendix A: Computation of natural variability indices

For the computation of pre-industrial natural variability indices we follow the procedure used by NOAA to calculate the indices employed in ClimaMeter.

The Niño 3.4 index is computed following the method by Bamston et al. (1997), based on monthly SSTs averaged over the Niño 3.4 region ([170°W; 120°W] x [5°N; 5°S], blue rectangle in Fig. A1). We compute SST monthly mean and standard deviation over the reference period, and remove the monthly seasonal cycle to get the anomalies. We finally standardize dividing by the monthly standard deviation.

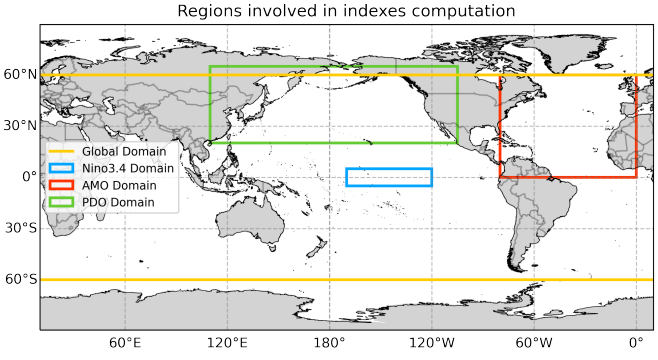

Figure A1. Regions involved in the ENSO, AMO, and PDO indices computation.

The AMO index is defined as the residual footprint of the SST anomalies after the removal of the externally forced signal. Residuals are defined as departures of local SST anomalies from the concurrent global-mean SST anomaly, namely the difference between local monthly SST anomalies in the North Atlantic and the monthly mean global average SST anomaly (Trenberth and Shea, 2006). The use of residual SST anomalies mitigates the influence of global-mean SST external trends on the quantification of natural variability Zhang et al. (1997). Operationally, we compute the monthly SST anomalies time series averaged over the North Atlantic region ([80°W; 0°E] x [60°N; 0°N], red rectangle in Fig. A1) and over the global oceans ([80°W; 180°E] x [60°N; 60°S]; yellow square in Fig. A1). The index is obtained by subtracting the global time series from the North Atlantic one.

The PDO index is defined as the leading principal component (PC) obtained from the empirical orthogonal function analysis of monthly residual SST anomalies poleward of 20°N in the Pacific Basin (Mantua and Hare, 2002). Residuals are defined as for AMO, but the local anomalies are computed on the North Pacific basin: we compute monthly SST anomalies in the North Pacific basin ([110°E; 255°E] x [65°N; 20°N], green rectangle in Fig. A1) and over the global oceans as for AMO, and then

https://doi.org/10.5194/egusphere-2026-1466
Preprint. Discussion started: 9 April 2026

subtract. We apply PC analysis to monthly residual SST anomalies. We select the first PC and we choose its sign so that it agrees with the definition of the positive phase of PDO: warm conditions in the central-eastern tropical Pacific surrounded by negative SST anomalies to the west of the basin (IPCC, 2021a). The index is finally obtained by dividing the first PC by the monthly standard deviation computed over the reference period for climatology Mantua et al. (1997).

The reference period for the climatology of the NOAA indices is the 30-year period from 1971 to 2000 (Xue et al., 2003).

Data availability. ERA5 (Hersbach et al., 2020) was downloaded from the Copernicus Climate Change Service (https://cds.climate.copernicus.eu/). We acknowledge the World Climate Research Programme's Working Group on Coupled Modelling, which is responsible for CMIP, and we thank the climate modeling groups for producing and making available their models outputs. For CMIP, the U.S. Department of Energy's Program for Climate Model Diagnosis and Intercomparison provides coordinating support and led development of software infrastructure in partnership with the Global Organization for Earth System Science Portals. The pre-industrial simulations of the three models were retrieved from the IPSL cluster. The Niño 3.4 and the AMO indices were retrieved from the Royal Netherlands Meteorological Institute Climate Explorer (https://climexp.knmi.nl/selectindex.cgi?id=someone@somewhere), while the PDO index from the National Centers for Environmental Information website (https://www.ncei.noaa.gov/pub/data/cmb/ersst/v5/index/ersst.v5.pdo.dat).

Author contributions. MV developed the main extension of the methodology, which was refined and implemented by CN. CN performed the computations and all the tests and created the figures. All authors contributed to the analyses and the discussion of the results. CN wrote the article with inputs from all the co-authors.

Competing interests. The authors declare that they have no conflict of interest.

Acknowledgements. This work benefited from state aid managed by the National Research Agency under France 2030, bearing the references ANR-22-EXTR-0005 (TRACCS-PC4-EXTENDING project), and has received funding from Autorité de sûreté nucléaire et de radioprotection (ASNR). CN and MV acknowledge the support of the INRAE / Mines Paris chair "Geolearning". We also acknowledge the useful discussions and comments of Pascal Yiou, Flavio Pons, Lucas Fery, and all the ClimaMeter team members (see the website https://www.climameter.org/consortium for the full list).

https://doi.org/10.5194/egusphere-2026-1466
Preprint. Discussion started: 9 April 2026

References

Alberti, T. and Faranda, D.: Strong winds in storm Ciarán likely influenced by both human-driven climate change and natural variability, https://doi.org/10.5281/zenodo.14164604, 2024.

Allen, M.: In defense of the traditional null hypothesis: remarks on the Trenberth and Curry WIREs opinion articles, WIREs Climate Change, 2, 931–934, https://doi.org/https://doi.org/10.1002/wcc.145, 2011.

Anderson, T. W.: On the Distribution of the Two-Sample Cramér-von Mises Criterion, The Annals of Mathematical Statistics, 33, 1148–1159, 1962.

Bamston, A., Chelliah, M., and Goldenberg, S.: Documentation of a highly ENSO-related SST region in the Equatorial Pacific, Atmosphere-Ocean, 35, 367–383, https://doi.org/10.1080/07055900.1997.9649597, 1997.

Bell, B., Hersbach, H., Simmons, A., Berrisford, P., Dahlgren, P., Horányi, A., Muñoz-Sabater, J., Nicolas, J., Radu, R., Schepers, D., Soci, C., Villaume, S., Bidlot, J.-R., Haimberger, L., Woollen, J., Buontempo, C., and Thépaut, J.-N.: The ERA5 global reanalysis: Preliminary extension to 1950, Quarterly Journal of the Royal Meteorological Society, 147, 4186–4227, https://doi.org/https://doi.org/10.1002/qj.4174, 2021.

Bellomo, K., Murphy, L., Cane, M., Clement, A., and Polvani, L.: Historical forcings as main drivers of the Atlantic multidecadal variability in the CESM large ensemble, Climate Dynamics, 50, 3687–3698, https://doi.org/10.1007/s00382-017-3834-3, 2018.

Birkel, S., Mayewski, P., Maasch, K., Kurbatov, A., and Lyon, B.: Evidence for a volcanic underpinning of the Atlantic multidecadal oscillation, npj Climate and Atmospheric Science, 1, https://doi.org/10.1038/s41612-018-0036-6, 2018.

Bonnet, R., Boucher, O., Deshayes, J., Gastineau, G., Hourdin, F., Mignot, J., Servonnat, J., and Swingedouw, D.: Presentation and Evaluation of the IPSL-CM6A-LR Ensemble of Extended Historical Simulations, Journal of Advances in Modeling Earth Systems, 13, e2021MS002 565, https://doi.org/https://doi.org/10.1029/2021MS002565, e2021MS002565 2021MS002565, 2021.

Boucher, O., Servonnat, J., Albright, A. L., Aumont, O., Balkanski, Y., Bastrikov, V., Bekki, S., Bonnet, R., Bony, S., Bopp, L., Braconnot, P., Brockmann, P., Cadule, P., Caubel, A., Cheruy, F., Codron, F., Cozic, A., Cugnet, D., D'Andrea, F., Davini, P., de Lavergne, C., Denvil, S., Deshayes, J., Devilliers, M., Ducharne, A., Dufresne, J.-L., Dupont, E., Éthé, C., Fairhead, L., Falletti, L., Flavoni, S., Foujols, M.-A., Gardoll, S., Gastineau, G., Ghattas, J., Grandpeix, J.-Y., Guenet, B., Guez, Lionel, E., Guilyardi, E., Guimberteau, M., Hauglustaine, D., Hourdin, F., Idelkadi, A., Joussaume, S., Kageyama, M., Khodri, M., Krinner, G., Lebas, N., Levavasseur, G., Lévy, C., Li, L., Lott, F., Lurton, T., Luyssaert, S., Madec, G., Madeleine, J.-B., Maignan, F., Marchand, M., Marti, O., Mellul, L., Meurdesoif, Y., Mignot, J., Musat, I., Ottlé, C., Peylin, P., Planton, Y., Polcher, J., Rio, C., Rochetin, N., Rousset, C., Sepulchre, P., Sima, A., Swingedouw, D., Thiéblemont, R., Traore, A. K., Vancoppenolle, M., Vial, J., Vialard, J., Viovy, N., and Vuichard, N.: Presentation and Evaluation of the IPSL-CM6A-LR Climate Model, Journal of Advances in Modeling Earth Systems, 12, e2019MS002 010, https://doi.org/https://doi.org/10.1029/2019MS002010, e2019MS002010 10.1029/2019MS002010, 2020.

Bourdin, S., Camargo, S., Lee, C., Lin, J., Vrac, M., Vaittinada Ayar, P., and Faranda, D.: Improving analogues-based detection attribution approaches for hurricanes, Environmental Research Letters, 20, https://doi.org/10.1088/1748-9326/adaa8d, 2025.

Cattiaux, J., Vautard, R., Cassou, C., Yiou, P., Masson-Delmotte, V., and Codron, F.: Winter 2010 in Europe: A cold extreme in a warming climate, Geophysical Research Letters, 37, https://doi.org/10.1029/2010GL044613, 2010.

Christidis, N. and Stott, P. A.: Attribution analyses of temperature extremes using a set of 16 indices, Weather and Climate Extremes, 14, 24–35, https://doi.org/https://doi.org/10.1016/j.wace.2016.10.003, 2016.

https://doi.org/10.5194/egusphere-2026-1466
Preprint. Discussion started: 9 April 2026

Deser, C., Alexander, M., Xie, S.-P., and Phillips, A.: Sea Surface Temperature Variability: Patterns and Mechanisms, Annual review of marine science, 2, 115–43, https://doi.org/10.1146/annurev-marine-120408-151453, 2010.

Dong, C., Noyelle, R., Messori, G., Gualandi, A., Fery, L., Yiou, P., Vrac, M., D'Andrea, F., Camargo, S. J., Coppola, E., Balsamo, G., Chen, C., Faranda, D., and Mengaldo, G.: Indo-Pacific regional extremes aggravated by changes in tropical weather patterns, Nature Geoscience, 17, 979–986, https://doi.org/10.1038/s41561-024-01537-8, publisher: Nature Publishing Group, 2024.

Douville, H., Raghavan, K., Renwick, J., Allan, R., Arias, P., Barlow, M., Cerezo-Mota, R., Cherchi, A., Gan, T., Gergis, J., Jiang, D., Khan, A., Pokam Mba, W., Rosenfeld, D., Tierney, J., and Zolina, O.: Water Cycle Changes, p. 1055–1210, Cambridge University Press, Cambridge, United Kingdom and New York, NY, USA, https://doi.org/10.1017/9781009157896.010, 2021.

ECMWF - Parameter Database: Mean sea level pressure - msl, https://codes.ecmwf.int/grib/param-db/151, a.

ECMWF - Parameter Database: 2 metre temperature - 2t, https://codes.ecmwf.int/grib/param-db/167, b.

ECMWF - Parameter Database: Total precipitation - tp, https://codes.ecmwf.int/grib/param-db/228, c.

ECMWF - Parameter Database: 10 metre U wind component - 10u, https://codes.ecmwf.int/grib/param-db/165, d.

ECMWF - Parameter Database: 10 metre V wind component - 10v, https://codes.ecmwf.int/grib/param-db/166, e.

Eyring, V., Bony, S., Meehl, G., Senior, C., Stevens, B., Ronald, S., and Taylor, K.: Overview of the Coupled Model Intercomparison Project Phase 6 (CMIP6) experimental design and organization, Geoscientific Model Development Discussions, 9, 1937–1958, https://doi.org/10.5194/gmd-9-1937-2016, 2016.

Eyring, V., Gillett, N., Achuta Rao, K., Barimalala, R., Barreiro Parrillo, M., Bellouin, N., Cassou, C., Durack, P., Kosaka, Y., McGregor, S., Min, S., Morgenstern, O., and Sun, Y.: Human Influence on the Climate System, p. 423–552, Cambridge University Press, Cambridge, United Kingdom and New York, NY, USA, https://doi.org/10.1017/9781009157896.005, 2021.

Faranda, D., Bourdin, S., Ginesta, M., Krouma, M., Noyelle, R., Pons, F., Yiou, P., and Messori, G.: A climate-change attribution retrospective of some impactful weather extremes of 2021, Weather and Climate Dynamics, 3, 1311–1340, https://doi.org/10.5194/wcd-3-1311-2022, 2022.

Faranda, D., Pascale, S., and Bulut, B.: Persistent anticyclonic conditions and climate change exacerbated the exceptional 2022 European-Mediterranean drought, Environmental Research Letters, 18, https://doi.org/10.1088/1748-9326/acbc37, 2023.

Faranda, D., Alberti, T., and Messori, G.: High temperatures in the 2023 September European heatwave enhanced by both human-driven climate change and natural variability, https://doi.org/10.5281/zenodo.14164864, 2024a.

Faranda, D., Messori, G., Coppola, E., Alberti, T., Vrac, M., Pons, F., Yiou, P., Saint Lu, M., Hisi, A. N. S., Brockmann, P., Dafis, S., Mengaldo, G., and Vautard, R.: ClimaMeter: contextualizing extreme weather in a changing climate, Weather and Climate Dynamics, 5, 959–983, https://doi.org/10.5194/wcd-5-959-2024, 2024b.

Fery, L. and Faranda, D.: Analysing 23 years of warm-season derechos in France: a climatology and investigation of synoptic and environmental changes, Weather and Climate Dynamics, 5, 439–461, https://doi.org/10.5194/wcd-5-439-2024, 2024.

Gavras-van Garderen, L., Feser, F., and Shepherd, T.: A methodology for attributing the role of climate change in extreme events: a global spectrally nudged storyline, Natural Hazards and Earth System Sciences, 21, 171–186, https://doi.org/10.5194/nhess-21-171-2021, 2021.

Ginesta, M., Yiou, P., Messori, G., and Faranda, D.: A methodology for attributing severe extratropical cyclones to climate change based on reanalysis data: the case study of storm Alex 2020, Climate Dynamics, 61, 1–25, https://doi.org/10.1007/s00382-022-06565-x, 2022.

Ginesta, M., Flaounas, E., Yiou, P., and Faranda, D.: Anthropogenic Climate Change Will Intensify European Explosive Storms Analogous to Alex, Eunice, and Xynthia, Journal of Climate, 37, 5427 – 5452, https://doi.org/10.1175/JCLI-D-23-0761.1, 2024.

https://doi.org/10.5194/egusphere-2026-1466
Preprint. Discussion started: 9 April 2026

Gulev, S., Thorne, P., Ahn, J., Dentener, F., Domingues, C., Gerland, S., Gong, D., Kaufman, D., Nnamchi, H., Quaas, J., Rivera, J., Sathyendranath, S., Smith, S., Trewin, B., von Schuckmann, K., and Vose, R.: Changing State of the Climate System, p. 287–422, Cambridge University Press, Cambridge, United Kingdom and New York, NY, USA, https://doi.org/10.1017/9781009157896.004, 2021.

Hartmann, D. L.: Appendix B: The Clausius-Clapeyron Relation, in: Global Physical Climatology, vol. 56 of *International Geophysics*, pp. 350–351, Academic Press, https://doi.org/https://doi.org/10.1016/S0074-6142(08)60571-9, 1994.

Henley, B. J.: Global and Planetary Change, 155, 42–55, https://doi.org/https://doi.org/10.1016/j.gloplacha.2017.06.004, 2017.

Hersbach, H., Bell, B., Berrisford, P., Hirahara, S., Horányi, A., Muñoz-Sabater, J., Nicolas, J., Peubey, C., Radu, R., Schepers, D., Simmons, A., Soci, C., Abdalla, S., Abellan, X., Balsamo, G., Bechtold, P., Biavati, G., Bidlot, J., Bonavita, M., De Chiara, G., Dahlgren, P., Dee, D., Diamantakis, M., Dragani, R., Flemming, J., Forbes, R., Fuentes, M., Geer, A., Haimberger, L., Healy, S., Hogan, R. J., Hólm, E., Janisková, M., Keeley, S., Laloyaux, P., Lopez, P., Lupu, C., Radnoti, G., de Rosnay, P., Rozum, I., Vamborg, F., Villaume, S., and Thépaut, J.-N.: The ERA5 global reanalysis, Quarterly Journal of the Royal Meteorological Society, 146, 1999–2049, https://doi.org/https://doi.org/10.1002/qj.3803, 2020.

Hong, J.-S., Yeh, S.-W., and Yang, Y.-M.: Interbasin Interactions between the Pacific and Atlantic Oceans Depending on the Phase of Pacific Decadal Oscillation and Atlantic Multidecadal Oscillation, Journal of Climate, 35, 2883 – 2894, https://doi.org/10.1175/JCLI-D-21-0408.1, 2022.

Huang, B., Thorne, P. W., Banzon, V. F., Boyer, T., Chepurin, G., Lawrimore, J. H., Menne, M. J., Smith, T. M., Vose, R. S., and Zhang, H.-M.: Extended Reconstructed Sea Surface Temperature, Version 5 (ERSSTv5): Upgrades, Validations, and Intercomparisons, Journal of Climate, 30, 8179 – 8205, https://doi.org/10.1175/JCLI-D-16-0836.1, 2017.

IPCC: Annex IV: Modes of Variability [Cassou, C., A. Cherchi, Y. Kosaka (eds.)], p. 2153–2192, Cambridge University Press, Cambridge, United Kingdom and New York, NY, USA, https://doi.org/10.1017/9781009157896.018, 2021a.

IPCC: Summary for Policymakers, p. 3-32, Cambridge University Press, Cambridge, United Kingdom and New York, NY, USA, https://doi.org/10.1017/9781009157896.001, 2021b.

Jiang, W., Gastineau, G., and Codron, F.: Multicentennial Variability Driven by Salinity Exchanges Between the Atlantic and the Arctic Ocean in a Coupled Climate Model, Journal of Advances in Modeling Earth Systems, 13, e2020MS002 366, https://doi.org/https://doi.org/10.1029/2020MS002366, e2020MS002366 2020MS002366, 2021.

Jézéquel, A., Depoues, V., Guillemot, H., Trolliet, M., Vanderlinden, J.-P., and Yiou, P.: Behind the veil of extreme event attribution, Climatic Change, 149, 1–17, https://doi.org/10.1007/s10584-018-2252-9, 2018.

Khaled, Z. E. and Mcheick, H.: Case studies of communications systems during harsh environments: A review of approaches, weaknesses, and limitations to improve quality of service, International Journal of Distributed Sensor Networks, 15, 1550147719829 960, https://doi.org/10.1177/1550147719829960, 2019.

KNMI Climate Explorer: https://climexp.knmi.nl/start.cgi.

Koenker, R. and Bassett, G.: Regression Quantiles, Econometrica, 46, 33–50, http://www.jstor.org/stable/1913643, 1978.

Kucharski, F. and Joshi, M. K.: Influence of tropical South Atlantic sea-surface temperatures on the Indian summer monsoon in CMIP5 models, Quarterly Journal of the Royal Meteorological Society, 143, 1351–1363, https://doi.org/https://doi.org/10.1002/qj.3009, 2017.

Li, Z., Zhang, W., Jin, F.-F., Stuecker, M., Sun, C., Levine, A., Xu, H., and Liu, C.: A robust relationship between multidecadal global warming rate variations and the Atlantic Multidecadal Variability, Climate Dynamics, 55, https://doi.org/10.1007/s00382-020-05362-8, 2020.

https://doi.org/10.5194/egusphere-2026-1466
Preprint. Discussion started: 9 April 2026

Liguori, G., Mcgregor, S., Arblaster, J., Singh, M., and Meehl, G.: A joint role for forced and internally-driven variability in the decadal modulation of global warming, Nature Communications, 11, https://doi.org/10.1038/s41467-020-17683-7, 2020.

Mantua, N. J. and Hare, S. R.: The Pacific Decadal Oscillation, Journal of Oceanography, 58, 35–44, https://api.semanticscholar.org/CorpusID:5307916, 2002.

Mantua, N. J., Hare, S. R., Zhang, Y., Wallace, J. M., and Francis, R.: A Pacific Interdecadal Climate Oscillation with Impacts on Salmon Production, Bulletin of the American Meteorological Society, 78, 1069–1079, https://api.semanticscholar.org/CorpusID:27418729, 1997.

Mauritsen, T., Bader, J., Becker, T., Behrens, J., Bittner, M., Brokopf, R., Brovkin, V., Claussen, M., Crueger, T., Esch, M., Fast, I., Fiedler, S., Fläschner, D., Gayler, V., Giorgetta, M., Goll, D. S., Haak, H., Hagemann, S., Hedemann, C., Hohenegger, C., Ilyina, T., Jahns, T., Jimenéz-de-la Cuesta, D., Jungclaus, J., Kleinen, T., Kloster, S., Kracher, D., Kinne, S., Kleberg, D., Lasslop, G., Kornblueh, L., Marotzke, J., Matei, D., Meraner, K., Mikolajewicz, U., Modali, K., Möbis, B., Müller, W. A., Nabel, J. E. M. S., Nam, C. C. W., Notz, D., Nyawira, S.-S., Paulsen, H., Peters, K., Pincus, R., Pohlmann, H., Pongratz, J., Popp, M., Raddatz, T. J., Rast, S., Redler, R., Reick, C. H., Rohrschneider, T., Schemann, V., Schmidt, H., Schnur, R., Schulzweida, U., Six, K. D., Stein, L., Stemmler, I., Stevens, B., von Storch, J.-S., Tian, F., Voigt, A., Vrese, P., Wieners, K.-H., Wilkenskjeld, S., Winkler, A., and Roeckner, E.: Developments in the MPI-M Earth System Model version 1.2 (MPI-ESM1.2) and Its Response to Increasing CO2, Journal of Advances in Modeling Earth Systems, 11, 998–1038, https://doi.org/https://doi.org/10.1029/2018MS001400, 2019.

Mcgregor, S., Timmermann, A., Stuecker, M., England, M., Merrifield, M., Jin, F.-F., and Chikamoto, Y.: Recent Walker circulation strengthening and Pacific cooling amplified by Atlantic warming, Nature Climate Change, https://doi.org/10.1038/NCLIMATE2330, 2014.

Meehl, G., Hu, A., Santer, B., and Xie, S.-P.: Contribution of the Interdecadal Pacific Oscillation to twentieth-century global surface temperature trends, Nature Climate Change, 6, https://doi.org/10.1038/nclimate3107, 2016.

Messori, G. and Faranda, D.: Heavy precipitation in storm Hans mostly strengthened by human-driven climate change and natural variability, https://doi.org/10.5281/zenodo.14169193, 2024.

METEO FRANCE: Ciarán and Domingos: France swept by two violent storms, https://meteofrance.com/actualites-et-dossiers/actualites/ciaran-et-domingos-la-france-balayee-par-deux-violentes-tempetes, a.

METEO FRANCE: Épisode de fortes chaleurs inédit pour septembre, https://meteofrance.com/actualites-et-dossiers/actualites/episode-de-fortes-chaleurs-tardif-et-durable-cette-semaine, b.

METEO FRANCE: Changement Climatique en France: les chiffres cles en 2024, https://meteofrance.com/le-changement-climatique/quel-climat-futur/changement-climatique-en-france-les-chiffres-cles-en, c.

Müller, W. A., Jungclaus, J. H., Mauritsen, T., Baehr, J., Bittner, M., Budich, R., Bunzel, F., Esch, M., Ghosh, R., Haak, H., Ilyina, T., Kleine, T., Kornblueh, L., Li, H., Modali, K., Notz, D., Pohlmann, H., Roeckner, E., Stemmler, I., Tian, F., and Marotzke, J.: A Higher-resolution Version of the Max Planck Institute Earth System Model (MPI-ESM1.2-HR), Journal of Advances in Modeling Earth Systems, 10, 1383–1413, https://doi.org/https://doi.org/10.1029/2017MS001217, 2018.

NCEI: https://www.ncei.noaa.gov/.

Nicolì, D., Bellucci, A., Iovino, D., Ruggieri, P., and Gualdi, S.: The impact of the AMV on Eurasian summer hydrological cycle, Scientific Reports, 10, 14 444, https://doi.org/10.1038/s41598-020-71464-2, 2020.

Otto, F.: Attribution of Weather and Climate Events, Annual Review of Environment and Resources, 42, https://doi.org/10.1146/annurev-environ-102016-060847, 2017.

Patricola, C. M., Saravanan, R., and Chang, P.: The Impact of the El Niño–Southern Oscillation and Atlantic Meridional Mode on Seasonal Atlantic Tropical Cyclone Activity, Journal of Climate, 27, 5311 – 5328, https://doi.org/10.1175/JCLI-D-13-00687.1, 2014.

https://doi.org/10.5194/egusphere-2026-1466
Preprint. Discussion started: 9 April 2026

Pfahl, S. and Wernli, H.: Quantifying the relevance of atmospheric blocking for co-located temperature extremes in the Northern Hemisphere on (sub-)daily time scales, Geophysical Research Letters, 39, https://doi.org/https://doi.org/10.1029/2012GL052261, 2012.

Seneviratne, S., Zhang, X., Adnan, M., Badi, W., Dereczynski, C., Di Luca, A., Ghosh, S., Iskandar, I., Kossin, J., Lewis, S., Otto, F., Pinto, I., Satoh, M., Vicente-Serrano, S., Wehner, M., and Zhou, B.: Weather and Climate Extreme Events in a Changing Climate, p. 1513–1766, Cambridge University Press, Cambridge, United Kingdom and New York, NY, USA, https://doi.org/10.1017/9781009157896.013, 2021.

Shepherd, T.: Atmospheric circulation as a source of uncertainty in climate change projections, Nature Geoscience, 7, 703–708, https://doi.org/10.1038/NGEO2253, 2014.

Shepherd, T.: A Common Framework for Approaches to Extreme Event Attribution, Current Climate Change Reports, 2, 28–38, https://doi.org/10.1007/s40641-016-0033-y, 2016.

Soubeyroux, J.-M., Dubuisson, B., Bernus, S., Samacoïts, R., Rousset, F., Schneider, M., Drouin, A., Madec, T., Tardy, M., and Corre, L.: A quel climat s'adapter en France selon la TRACC ?, Tech. rep., Meteo-France, https://hal.science/hal-04797481, 2024.

Sutton, R. and Dong, B.: Atlantic Ocean influence on a shift in European climate in the 1990s, Nature Geoscience, 5, 788–792, https://doi.org/10.1038/ngeo1595, 2012.

Swedish Meteorological and Hydrological Institute: August 2023 – Low pressure system Hans and record rainfall, https://www.smhi.se/klimat/klimatet-da-och-nu/manadens-vader-och-vatten-i-sverige/manadens-vader-och-vatten-i-sverige/2023-08-31-augusti-2023---lagtrycket-hans-och-rekordmycket-regn.

Trenberth, K., Fasullo, J., and Shepherd, T.: Attribution of climate extreme events, Nature Climate Change, 5, 725–730, https://doi.org/10.1038/nclimate2657, 2015.

Trenberth, K. E.: Attribution of climate variations and trends to human influences and natural variability, WIREs Climate Change, 2, 925–930, https://doi.org/https://doi.org/10.1002/wcc.142, 2011.

Trenberth, K. E. and Shea, D. J.: Atlantic hurricanes and natural variability in 2005, Geophysical Research Letters, 33, https://doi.org/https://doi.org/10.1029/2006GL026894, 2006.

Trenberth, K. E., Caron, J. M., Stepaniak, D. P., and Worley, S.: Evolution of El Niño–Southern Oscillation and global atmospheric surface temperatures, Journal of Geophysical Research: Atmospheres, 107, AAC 5–1–AAC 5–17, https://doi.org/https://doi.org/10.1029/2000JD000298, 2002.

Voldoire, A., Saint-Martin, D., Sénési, S., Decharme, B., Alias, A., Chevallier, M., Colin, J., Guérémy, J.-F., Michou, M., Moine, M.-P., Nabat, P., Roehrig, R., Salas y Mélia, D., Séférian, R., Valcke, S., Beau, I., Belamari, S., Berthet, S., Cassou, C., Cattiaux, J., Deshayes, J., Douville, H., Ethé, C., Franchistéguy, L., Geoffroy, O., Lévy, C., Madec, G., Meurdesoif, Y., Msadek, R., Ribes, A., Sanchez-Gomez, E., Terray, L., and Waldman, R.: Evaluation of CMIP6 DECK Experiments With CNRM-CM6-1, Journal of Advances in Modeling Earth Systems, 11, 2177–2213, https://doi.org/https://doi.org/10.1029/2019MS001683, 2019.

Wu, T., Hu, A., Gao, F., Zhang, J., and Meehl, G.: New insights into natural variability and anthropogenic forcing of global/regional climate evolution, npj Climate and Atmospheric Science, 2, https://doi.org/10.1038/s41612-019-0075-7, 2019.

Xue, Y., Smith, T. M., and Reynolds, R. W.: Interdecadal Changes of 30-Yr SST Normals during 1871–2000, Journal of Climate, 16, 1601 – 1612, https://doi.org/10.1175/1520-0442(2003)016<1601:ICOYSN>2.0.CO;2, 2003.

Yiou, P.: AnaWEGE: A weather generator based on analogues of atmospheric circulation, Geoscientific Model Development, 7, 531–543, https://doi.org/10.5194/gmd-7-531-2014, 2014.

https://doi.org/10.5194/egusphere-2026-1466
Preprint. Discussion started: 9 April 2026

Yiou, P., Vautard, R., Naveau, P., and Cassou, C.: Inconsistency between atmospheric dynamics and temperatures during the exceptional 2006/2007 fall/winter and recent warming in Europe, Geophysical Research Letters, 34, https://doi.org/https://doi.org/10.1029/2007GL031981, 2007.

Zanchettin, D., Rubino, A., Matei, D., Bothe, O., and Jungclaus, J.: Multidecadal-to-centennial SST variability in the MPI-ESM simulation ensemble for the last millennium, Climate Dynamics, 40, 1–18, https://doi.org/10.1007/s00382-012-1361-9, 2012.

Zhang, W., Vecchi, G., Villarini, G., Murakami, H., Rosati, A., Yang, X., Jia, L., and Zeng, F.: Modulation of Western North Pacific Tropical Cyclone Activity by the Atlantic Meridional Mode, Climate Dynamics, 48, https://doi.org/10.1007/s00382-016-3099-2, 2017.

Zhang, Y., Wallace, J. M., and Battisti, D. S.: ENSO-like Interdecadal Variability: 1900–93, Journal of Climate, 10, 1004 – 1020, https://doi.org/10.1175/1520-0442(1997)010<1004:ELIV>2.0.CO;2, 1997.